Applied Energy 424 (2026) 128445



Contents lists available at ScienceDirect

Applied Energy

journal homepage: www.elsevier.com/locate/apen

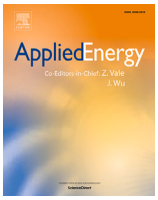

A decomposition method for optimizing the operation of power-to-X energy systems with detailed process models

Yifan Wang [a], Niklas von der Assen [a,*], Qi Zhang [b,*]

[a] Institute of Technical Thermodynamics, RWTH Aachen University, 52062 Aachen, Germany
[b] Department of Chemical Engineering and Materials Science, University of Minnesota, Minneapolis, MN 55455, USA

HIGHLIGHTS

- Operational optimization of renewables-based integrated energy systems.
- Decomposition method for problems with difficult-to-evaluate constraints.
- A surrogate modeling approach for multistage process systems.
- Three solution approaches for decomposed optimization problems solved within 1h.
- Application to a real-world power-to-X system with PEM, DAC, and methanation processes.

ARTICLE INFO

Keywords:
Renewables-based energy systems
Multistage process systems
PEM electrolyzer
Direct air capture plant
Methanation process
Surrogate model
MIQCQP

ABSTRACT

The growing reliance on renewable energy necessitates extending energy systems with complex processes such as power-to-X. Due to the diverse operational characteristics of these processes, the corresponding optimization problems are highly complex and result in models that are computationally difficult to solve. To address this computational challenge, this work proposes a decomposition method to solve operational optimization problems for complex energy systems with detailed process models. The method decomposes the original optimization problem into optimization problems with different levels of model granularity by incorporating a surrogate model for each process. Building on prior work focusing on a single continuous process system, this method is expanded to handle multiple and more complex process systems. To this end, we introduce a surrogate modeling approach for multistage process systems and develop three solution approaches for the operational optimization problems. The method is applied to minimize the daily operational cost of a real-world adapted power-to-X energy system with detailed process models of a PEM electrolyzer, a direct air capture plant and two methanation processes. All three solution approaches yield comparable operational costs, but differ in computational efficiency. The most efficient solution approach identifies an optimal operational strategy in under one hour. Additionally, a sensitivity study evaluates the impact of key parameters on the performance of the method, demonstrating its robustness and adaptability. The results highlight the potential of the proposed method to efficiently optimize the operations of complex integrated energy systems with detailed process models.

1. Introduction

Increased penetration of renewable energy sources calls for innovation in energy systems, including seasonal energy storage and supply [1–3], energy transport [4], alternative energy carriers [5–8], and highly dynamic operation [9]. These requirements lead to an integration of new and complex process systems into energy systems. In this context, power-to-X technologies play a central role. They encompass a broad spectrum of processes with diverse operational characteristics, such as electrolyzers and fuel cells [1,10], carbon capture plants [11], and various chemical synthesis processes, including the Sabatier reaction [12], Haber-Bosch process [6], and Fischer–Tropsch synthesis [13]. These novel energy systems are being explored in various research and demonstration projects, ranging from stand-alone technologies, local and residential applications, to industrial and national energy supply solutions [9,13,14].

Despite their high potential for defossilization, renewables-based energy systems can pose significant operational challenges, to a large

* Corresponding author.
Email addresses: yifan.wang@ltt.rwth-aachen.de (Y. Wang), niklas.vonderassen@ltt.rwth-aachen.de (N. von der Assen), qizh@umn.edu (Q. Zhang).

https://doi.org/10.1016/j.apenergy.2026.128445
Received 17 April 2026; Received in revised form 25 June 2026; Accepted 10 July 2026
Available online 21 July 2026
0306-2619/© 2026 The Author(s). Published by Elsevier Ltd. This is an open access article under the CC BY license (http://creativecommons.org/licenses/by/4.0/).

extent due to the heterogeneity in operational characteristics across the different involved process systems. For example, electrolyzers and fuel cells introduce electrochemical reactions into energy systems and allow rapid adjustment of production rates, but are coupled with slow temperature dynamics [15,16]; CO_2 direct air capture plants usually utilize adsorption–desorption processes, incorporating batch operations into energy systems [17]; chemical processes involve chemical reactions, where the catalysts used are often sensitive to the reaction temperature, limiting the flexibility of their operation [12]; and highly integrated or intensified processes pose challenges from a control standpoint [18,19]. Harmonizing the dynamic operation of such a diverse set of processes within a highly integrated energy system is a daunting task.

From a modeling standpoint, a major challenge in optimizing the operation of such energy systems arises from the highly nonlinear and nonconvex process models. Moreover, the operational decisions are typically made at discrete time steps throughout the considered time horizon, where the time resolution is primarily determined by the electricity price and energy demand profiles, which often leads to very large optimization problems. The model complexity further increases as we try to capture process dynamics, where even at the coarse-grained level, one needs to consider transitions between different operating states and constraints on the timing and duration of such transitions.

The operational optimization problems of the aforementioned energy systems have received increased attention in recent publications. Table 1 provides an overview of selected related studies.

Zhang and Zhang [11] presented a coupling model for the optimal scheduling of integrated energy systems, incorporating power-to-gas technologies and carbon capture power plants. Cheng et al. [20] proposed a new operational model for multi-carrier energy systems, considering power-to-gas technologies and CO_2-based electrothermal energy storage. Wu and Li [21] developed an optimal operation framework that integrates refined power-to-gas and carbon capture systems under carbon trading. In these works, complex process systems are modeled using simple input–output relationships. The operational performance of a process system is often captured in a single constant efficiency number, which is in most cases a drastic simplification. As a result, these simplified models are computationally efficient but may lead to suboptimal or infeasible decisions.

Table 1
Overview of existing literature for addressing operational optimization for renewables-based energy systems.

Category	Representative studies	Strengths (+) / Limitations (–)
Model simplifications		
constant efficiencies, linear regression models	[11], [20], [21],	+ easy implementation + low computational effort – reduced model fidelity – potential infeasibility
Advanced/detailed modeling approaches		
linear scale-bridging, dynamic ramping constraints	[16,22–24], [25],	+ high modeling accuracy + computational tractability
	[26]	– process-specific formulations – limited scalability
Advanced solution approaches		
dual-based decomposition	[27],	+ suitable for large-scale systems
	[28]	+ computational tractability – not applicable for difficult-to-evaluate models
bilevel decomposition	[29], [30], [28]	+ handles complex constraints + rigorous optimality – requiring integer cut; not suitable for detailed process models
Our previous work		
surrogate model-based decomposition	[31]	+ applicable for difficult-to-evaluate constraints + high scalability + computational tractability + ensures feasible optimal solutions – limited to a single continuous process

Other works have analyzed the detailed performance of specific processes and have applied more advanced techniques to model their complex operational characteristics. Baader et al. [22] proposed a scheduling approach that incorporates linear scale-bridging and data-driven models into an overall mixed-integer linear programming (MILP) formulation. Baader et al. [16,23,24] used dynamic ramping constraints to capture high-order dynamics of reactor and electrolyzer operations. However, these efforts focus on demand response problems and are primarily applicable to energy systems with short time horizons and specific processes. Bornemann et al. [25] optimized the operation of a PEM electrolyzer, including its downstream compression system, through a detailed process model. Their study underscored the notable economic and system efficiency benefits of employing detailed process models at the system scale. Papadimitriou et al. [26] compared high-fidelity models with local optimization versus surrogate models with global optimization for the dynamic scheduling of an air separation process, demonstrating that deterministic global dynamic optimization based on linear surrogate models often incurs infeasibility.

In short, addressing operational optimization problems for highly integrated renewables-based energy systems that involve complex process systems necessitates detailed process models to ensure operational feasibility. Such detailed process models may originate from computationally intensive finite element simulations, or comprehensive black-box models, or other numerically demanding formulations. Due to their complexity and limited analytical accessibility, these models cannot be directly embedded into standard optimization frameworks, thereby requiring the use of decomposition techniques [32,33].

A range of well-established decomposition methods for energy system optimization problems can be found in the literature, including dual-based approaches such as Dantzig-Wolfe decomposition, Lagrangian decomposition, ADMM, and Benders decomposition, as well as their various extensions and variants [28,32,33]. These decomposition techniques primarily address computational complexities arising from spatial and/or temporal coupling, i.e., from complicating (linking) constraints and variables [27,28]. Therefore, they are not directly suited to handle the type of computational complexity considered here, which stems from difficult-to-evaluate detailed process models.

Iyer and Grossmann [34] first proposed a bilevel decomposition method to address the combinatorial complexity of MILP problems while guaranteeing global optimality. The central idea is to reformulate the original optimization problem into two problems: a master problem and a subproblem. While the master problem represents a relaxed version of the original problem, the subproblem is a fixed version of the original problem, conditioned on the integer decision variables obtained from the master problem [34]. Because bilevel decomposition relies on integer decisions obtained in the master problem to define the subproblem, it has mostly been applied to synthesis problems, such as Jiménez-Romero et al. [30] and Elsido et al. [29]. Nevertheless, its decomposition structure, based on fixing and relaxing key decision variables, provides a means to handle complex constraints via separate subproblems.

Building on a similar decomposition structure, our previous work [31] introduced a decomposition method to identify optimal operational decisions for energy systems involving complex process systems. The proposed method models a complex process system using two levels of granularity: a detailed process model at the process system level and a corresponding surrogate process model at the energy system level. The two levels are coordinated through an iterative optimization approach. First, the optimization model at the energy system level determines the operational decisions. These operational decisions are then evaluated by the optimization model at the process system level to verify their feasibility. If deemed infeasible, the model at the energy system level

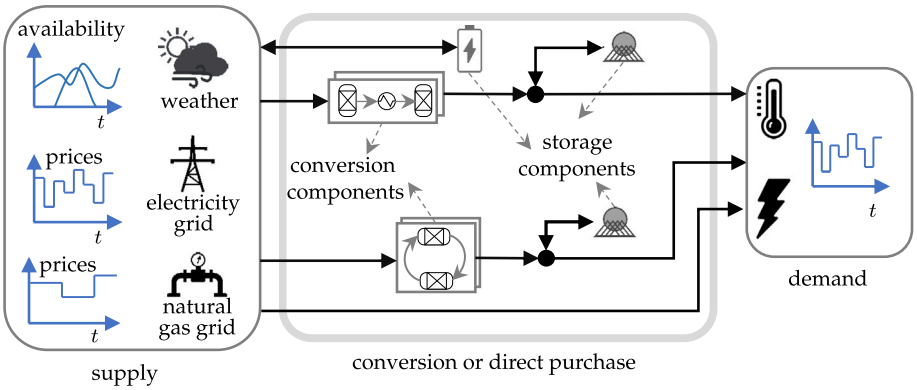

Fig. 1. Schematic illustration of the general structure of a renewables-based energy system.

is re-solved with updated penalty parameters. The algorithm continues until the energy system level proposes an operational strategy that is feasible at the process system level. The previous method was successfully applied to optimize the daily operation of a power-to-gas energy system involving a detailed methanation process model; however, it is restricted to energy systems employing a single continuous process model.

Overall, as summarized in Table 1, despite the growing interest, operational optimization problems of renewables-based energy systems still demand methods that can efficiently handle heterogeneous and difficult-to-evaluate detailed process models. To address this gap, in this work, we extend our previously proposed decomposition method to handle energy systems with multiple and more complex process models. First, we introduce a surrogate modeling approach tailored to multistage process systems, which significantly expands the capability of the energy system model. We then develop a similar decomposition structure that iterates between solving the energy system model and multiple detailed process models.

The remainder of this article is structured as follows: Section 2 provides a generic mathematical formulation of the operational optimization problem. Section 3 describes the proposed decomposition method in detail. In Section 4, we apply the proposed method to a real-world power-to-X energy system. In Section 5, we close with concluding remarks. The code for the implementation of the developed method, including all data for the case study, is publicly available at: https://git-ce.rwth-aachen.de/ltt/ptg-es4.

2. Generic mathematical formulation

A general structure of a renewables-based energy system is shown in Fig. 1, comprising different energy conversion and storage components. Various energy demands can be covered through on-site energy conversion and/or by direct purchase from the external supply. Both the supply and demand sides are subject to volatility due to fluctuations in renewable energy availability, energy prices, and consumption patterns.

The operational optimization problem for such energy systems has the following general form:

$$\min_{\dot{\boldsymbol{E}}^{\text{buy}},\dot{\boldsymbol{E}}^{\text{sell}},\dot{\boldsymbol{E}}^{\text{in}},\dot{\boldsymbol{E}}^{\text{out}},\boldsymbol{d}^{\text{PS}},\boldsymbol{x}^{\text{ES}}} \quad C = \sum_{t\in\mathcal{T}} \Delta t_t \sum_{\tilde{e}\in\mathcal{E}^{\text{ext}}} \left(c^{\text{buy}}_{\tilde{e},t}\dot{E}^{\text{buy}}_{\tilde{e},t} - c^{\text{sell}}_{\tilde{e},t}\dot{E}^{\text{sell}}_{\tilde{e},t} \right) \tag{1a}$$

s.t.

$$\sum_{k\in\mathcal{K}} \left(\dot{E}^{\text{out}}_{k,e,t} - \dot{E}^{\text{in}}_{k,e,t} \right) + \dot{E}^{\text{buy}}_{e,t} - \dot{E}^{\text{sell}}_{e,t} = \dot{E}^{\text{D}}_{e,t} \qquad \forall e\in\mathcal{E}, t\in\mathcal{T}, \tag{1b}$$

$$\boldsymbol{g}(\dot{\boldsymbol{E}}^{\text{in}}_k, \dot{\boldsymbol{E}}^{\text{out}}_k, \boldsymbol{d}^{\text{PS}}_k, \boldsymbol{x}^{\text{ES}}) \le 0 \qquad \forall k\in\mathcal{K}, \tag{1c}$$

$$\dot{E}^{\text{buy}}_{e,t}, \dot{E}^{\text{sell}}_{e,t}, \dot{E}^{\text{in}}_{k,e,t}, \dot{E}^{\text{out}}_{k,e,t} \in \mathbb{R}^{+} \qquad \forall k\in\mathcal{K}, e\in\mathcal{E}, t\in\mathcal{T}, \tag{1d}$$

$$\boldsymbol{d}^{\text{PS}}_k \in \mathcal{D}_k \subset \mathbb{R}^{N_{\boldsymbol{d}^{\text{PS}}_k}} \qquad \forall k\in\mathcal{K}, \tag{1e}$$

$$\boldsymbol{x}^{\text{ES}} \in \mathbb{R}^{N_{\boldsymbol{x}^{\text{ES}}}}, \tag{1f}$$

where the goal is to minimize the operational cost C (Eq. (1a)) while fulfilling the energy demands $\dot{E}^{\text{D}}_{e,t}$ for each product e ($e\in\mathcal{E}$) at every time step t ($t\in\mathcal{T}$) via energy conversion or purchase from external energy supplies (Eq. (1b)). Here, Δt_t is the duration of time step t. $\mathcal{E}^{\text{ext}}$ is the set of all external energy forms with price parameters for buying ($c^{\text{buy}}_{\tilde{e},t}$) and selling ($c^{\text{sell}}_{\tilde{e},t}$). The set $\mathcal{K}$ contains all energy system components. For a component k, $\dot{E}^{\text{in}}_{k,e,t}$ and $\dot{E}^{\text{out}}_{k,e,t}$ represent the input and output flow of product e at time step t, respectively. Eq. (1c) represents all other constraints in a compact way, encompassing operational performance relationships and accounting for every energy system component $k\in\mathcal{K}$. All decision variables are summarized in Eqs. (1d), (1e) and (1f). The surrogate vectors $\boldsymbol{d}^{\text{PS}}$ and $\boldsymbol{x}^{\text{ES}}$ represent other decision variables that are not explicitly specified here in a general manner. The vector $\boldsymbol{d}^{\text{PS}}_k$ collects all decision variables within the detailed process model of energy system component k, e.g., reactor inlet temperature or compressor outlet pressure. In contrast, $\boldsymbol{x}^{\text{ES}}$ contains decision variables at the coarse-grained model level, such as on/off decisions of conversion components and charge/discharge decisions of storage components.

For notational convenience, we adopt the following convention: Given a decision variable indexed over multiple sets, say $x_{k,e,t}$ with $k\in\mathcal{K}$, $e\in\mathcal{E}$, and $t\in\mathcal{T}$, the bold notation $\boldsymbol{x}_k$ or $\boldsymbol{x}$ represents the vector containing all $x_{k,e,t}$ over subsets or the entire index set. For example, $\dot{\boldsymbol{E}}^{\text{in}}_{k,t}$ denotes $\dot{E}^{\text{in}}_{k,e,t}, \forall e\in\mathcal{E}$; $\dot{\boldsymbol{E}}^{\text{in}}$ represents $\dot{E}^{\text{in}}_{k,e,t}, \forall k\in\mathcal{K}, e\in\mathcal{E}, t\in\mathcal{T}$. Additionally, "&" and "/" in the superscript represent the union and selection between two decision variables, respectively. For instance, $\dot{E}^{\text{in\&out}}_{k,e,t}$ denotes the union of $\dot{E}^{\text{in}}_{k,e,t}$ and $\dot{E}^{\text{out}}_{k,e,t}$; $\dot{E}^{\text{in/out}}_{k,e,t}$ indicates the decision variable $\dot{E}^{\text{in}}_{k,e,t}$ or $\dot{E}^{\text{out}}_{k,e,t}$.

Typically, constraint Eq. (1c) is simplified to a linear input–output relationship for a given energy system component k across all time steps, with the vector $\boldsymbol{d}^{\text{PS}}_k$ being empty. Such simplification can lead to infeasible operational decisions. Thus, this work addresses the operational optimization problem with a focus on energy system components that necessitate detailed process models. For clarity, we collect these energy system components in the set $\mathcal{K}^{\text{PS}}$ ($\mathcal{K}^{\text{PS}}\subseteq\mathcal{K}$), and the corresponding detailed process models are included in constraint Eq. (1c).

3. Decomposition method

The present decomposition method builds on our previous work [31], designed to solve Problem (1). As presented in the overview in Fig. 2, the method decomposes Problem (1) into one optimization problem at the energy system level (denoted by the superscript ES) and multiple optimization problems at the process system level (denoted by the superscript PS). At the energy system level, the detailed process models are replaced with simpler surrogate models, while the full detailed process models are considered at the process system level.

The decomposition method consists of seven steps, divided into two parts: Part A prepares the models for Part B, where the operational optimization takes place. The main idea in Part B is to iterate between

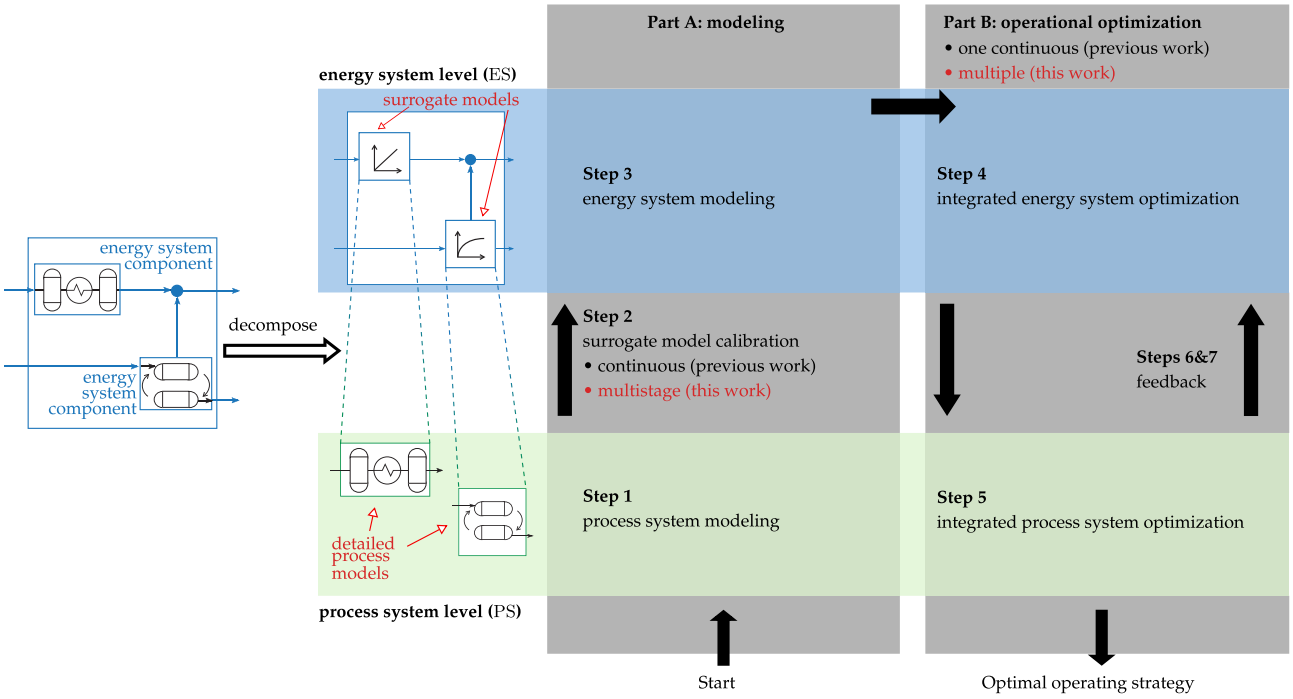

Fig. 2. Schematic illustration of the decomposition method, building upon our previous work [31]. The key idea is to decompose Problem (1) into an optimization problem at the energy system level and multiple optimization problems at the process system level. The proposed method consists of seven steps, divided into two parts: In Part A, models with two different levels of granularity are prepared, and in Part B, the resulting operational optimization problems are solved iteratively.

the energy and the process system models where convergence is achieved by updating a penalty term at the energy system level. We briefly outline the key concepts underlying each step here. Detailed explanations and the implementation of the extensions introduced in this work (highlighted in red in Fig. 2) are presented in the following subsections. For additional details, readers are referred to Wang et al. [31].

Part A consists of three steps (Steps 1 to 3). Step 1 focuses on detailed process system modeling of each energy system component k ($k \in \mathcal{K}^{\mathrm{PS}}$). Here, we can consider various types of process models, including those that are practically black boxes; the main requirement is that the model returns optimal or near-optimal operational decisions given a specified model input. In Step 2, we generate data by running the process models for different input values and utilize these datasets to develop simpler surrogate models, which are then incorporated into the energy system model in Step 3.

Part B consists of four steps (Steps 4 to 7). We begin by solving the optimization problem with lower-granularity surrogate models at the energy system level in Step 4 to determine the optimal operational decisions for each energy system component. The optimal operational decisions for each component k ($k \in \mathcal{K}^{\mathrm{PS}}$) are then passed to the process system level, where their feasibility is evaluated using the detailed process models in Step 5. If any infeasibility arises, information is sent back to the energy system level through Steps 6 and 7. Step 6 provides estimated operational costs at the process system level. This step can be skipped if the operational costs are already embedded in the surrogate models. Step 7 identifies the time steps where infeasibility occurs at the process system level and determines which decision variables should be penalized at the energy system level in subsequent iterations. We then return to Step 4, where the operational optimization problem at the energy system level, along with the estimation and penalty information from the previous iteration at the process system level, is re-solved. This iterative communication between the two levels continues until we converge on a consistent set of operational decisions or the maximum number of iterations is reached. If the latter occurs, the operational problem is deemed infeasible; we discuss this scenario later in this section.

In our previous work, we only considered a simple continuous process system with the assumption that, given appropriate ramping constraints, steady-state operation could always be reached within a fraction of the length of one time step (cf. Δt_t in Problem (1)). In this work, we extend Part A to incorporate more complex process systems, including batch plants that involve multiple intricate processing stages (hereafter referred to as multistage process systems for brevity), and advance Part B to address the instances involving multiple process systems.

3.1. Part A: modeling

Part A prepares mathematical models for a given energy system; it includes process system modeling (Step 1), surrogate model calibration (Step 2), and energy system modeling (Step 3) (cf. the middle part in Fig. 2). Using the detailed process models from Step 1, we generate a dataset $DS_{k,e}$, which contains (near-)optimal operational decisions for each energy system component k with a representative product e. We then utilize the dataset $DS_{k,e}$ to construct a surrogate model for each process k.

We generally assume that a process needs to go through "cycles," where a cycle is defined as a given sequence of consecutive processing and transition stages, which we refer to as "segments." Fig. 3 shows an example where three time steps, each corresponding to one segment, are required to complete a cycle. Here, the process operates during the first three time steps, with segment s_1 active at t_1, s_2 at t_2, and s_3 at t_3. After completing its cycle, the process system is turned off at time step t_4. We introduce the binary variable $\alpha_{s,t}$ to represent the active/inactive status of segment s at time step t, and the binary variable β_t to indicate the on/off status of the process system at time step t. In the simplest case of a continuous process operating at steady state, its cycle has only one segment.

For a given process, $S = \{s_1, s_2, \ldots, s_{\mathrm{N}}\}$ denotes the ordered set of segments required to complete a full cycle. The surrogate model for the process is constructed as follows, with a corresponding illustration shown in Table 2. For clarity, we use the surrogate decision variables

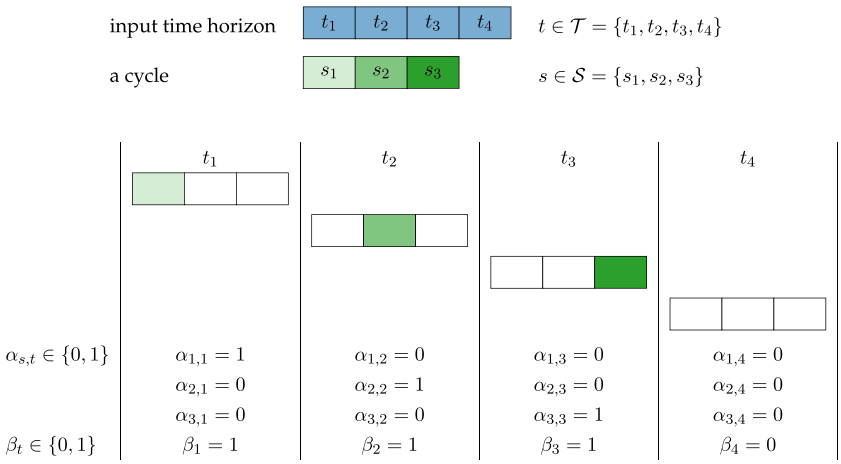

Fig. 3. Illustrative example where a cycle of the process system is completed during the first three time steps of the given time horizon.

Table 2
Illustration of the surrogate modeling approach for process systems.

Description	Graphical illustration	Surrogate model
each segment at every time step $\forall s \in \mathcal{S}, t \in \mathcal{T}$	$x_{s,t}$ … $y_{s,t}$	Eqs. (2a) to (2c)
each time step $\forall t \in \mathcal{T}$	$\beta_t, \bar{x}_t$; $\alpha_{s_1,t}\, x_{s_1,t}$ $\alpha_{s_2,t}\, x_{s_2,t}$ $\alpha_{s,t}\, x_{s,t}$ $\alpha_{s_N,t}\, x_{s_N,t}$; $y_{s_1,t}$ $y_{s_2,t}$ $y_{s,t}$ $y_{s_N,t}$; $\bar{y}_t$	Eqs. (3a) to (3c)
every two adjacent time steps $\forall t, t+1 \in \mathcal{T}$	t $t+1$	Eqs. (4a) to (4c)
every $\lvert\mathcal{S}\rvert$ consecutive time steps (a cycle) $\forall t, t+1, \ldots, t+\lvert\mathcal{S}\rvert-1 \in \mathcal{T}$	t $t+1$; $x_{s_1,t}$ $x_{s_2,t+1}$; $y_{s_1,t}$ $y_{s_2,t+1}$; … $t+\lvert\mathcal{S}\rvert-1$; $x_{s,\ldots}$ $x_{s_N,t+\lvert\mathcal{S}\rvert-1}$; $y_{s,\ldots}$ $y_{s_N,t+\lvert\mathcal{S}\rvert-1}$	Eqs. (5a) and (5b)

x and y to generally represent the input and output product flows of the given process, respectively. Note that these definitions differ slightly from those stated in the original optimization problem (Problem (1)).

For each segment (cf. the second row in Table 2), input–output relationships are fitted using the dataset created in Step 2; these relationships are captured in Eq. (2a). Furthermore, x and y are constrained by their respective bounds when the corresponding segment is active (Eqs. (2b) and (2c)).

$$y_{s,t} = f(x_{s,t}) \qquad \forall s \in S, t \in \mathcal{T}, \tag{2a}$$

$$\alpha_{s,t} x^{\min}_{s,t} \le x_{s,t} \le \alpha_{s,t} x^{\max}_{s,t} \qquad \forall s \in S, t \in \mathcal{T}, \tag{2b}$$

$$\alpha_{s,t} y^{\min}_{s,t} \le y_{s,t} \le \alpha_{s,t} y^{\max}_{s,t} \qquad \forall s \in S, t \in \mathcal{T}. \tag{2c}$$

As illustrated in the third row of Table 2, the following constraints ensure that no more than one segment can be selected at each time step (Eq. (3a)) and define aggregate variables $\bar{x}_t$ and $\bar{y}_t$ that represent the input and output variables, respectively, at each time step (Eqs. (3b) and (3c)).

$$\beta_t = \sum_{s\in S} \alpha_{s,t} \qquad \forall t \in \mathcal{T}, \tag{3a}$$

$$\bar{x}_t = \sum_{s\in S} x_{s,t} \qquad \forall t \in \mathcal{T}, \tag{3b}$$

$$\bar{y}_t = \sum_{s\in S} y_{s,t} \qquad \forall t \in \mathcal{T}. \tag{3c}$$

Considering the connectivity of segments within a cycle, as shown in the fourth row of Table 2, if the first segment s_1 is activated at time step t, the subsequent $|S|-1$ segments are also activated at the following time steps (Eq. (4a)). Eqs. (4b) and (4c) further ensure that there are no partial cycles within the given time horizon $\mathcal{T} = \{t_1, t_2, \dots, t_{\text{end}}\}$.

$$\alpha_{s,t} = \alpha_{s+1,t+1} \qquad \forall s \in S\backslash\{s_N\}, t \in \mathcal{T}\backslash\{t_1, t_{\text{end}}\}, \tag{4a}$$

$$\alpha_{s,t_1} = 0 \qquad \forall s \in S\backslash\{s_1\}, \tag{4b}$$

$$\alpha_{s,t_{\text{end}}} = 0 \qquad \forall s \in S\backslash\{s_N\}. \tag{4c}$$

Furthermore, as depicted in the last row of Table 2, additional constraints are introduced to represent the interdependence among the different segments (Eq. (5a)). Based on our modeling approach, this interdependence is best represented at the cycle domain, to be precise, over every $|S|$ consecutive time steps. The output variable of each segment within a cycle relates to the overall input variables of that cycle, which are distributed across the time steps from t to $t+|S|-1$ (Eq. (5b)).

$$l_{s,t} = f(x_{s_1,t}, \dots, x_{s,t}, \dots, x_{s_N,t}) \qquad \forall t \in \mathcal{T}, \tag{5a}$$

$$0 = \alpha_{s_1,t} \sum_{\tilde{t}=t}^{t+|S|-1} (y_{s,\tilde{t}} - l_{s,\tilde{t}}) \qquad \forall s \in S, t \in \mathcal{T}\backslash\{t_{\text{end}} - |S| + 2, \dots, t_{\text{end}}\}. \tag{5b}$$

In this way, we decompose the production cycle of a multistage process system into multiple segments to align its time resolution with that of the energy system. The operational performance of the process is then approximated via its surrogate model Eqs. (2) to (5), while the input–output relationships are captured in Eqs. (2) and (5).

The exact formulations of Eqs. (2a) and (5a) can be obtained using any suitable surrogate model, such as linear regression, based on the distribution of operational data collected in the dataset $\mathcal{DS}_{k,e}$. In addition, time step t in Eq. (5b) aligns with Eqs. (4b) and (4c). If partial cycles within $\mathcal{T}$ are considered, constraints Eqs. (4b), (4c) and (5b) should be updated accordingly.

With the modeling of the production cycles shown above and the corresponding surrogate models, we can formulate a simplified energy system model in the following general form:

$$\min_{\dot{\boldsymbol{E}}^{\text{buy,ES}}, \dot{\boldsymbol{E}}^{\text{sell,ES}}, \dot{\boldsymbol{E}}^{\text{in,ES}}, \dot{\boldsymbol{E}}^{\text{out,ES}}, \boldsymbol{x}^{\text{ES}}} C^{\text{ES}} = \sum_{t\in\mathcal{T}} \Delta t_t \sum_{\tilde{e}\in\mathcal{E}^{\text{ext}}} \left(c^{\text{buy}}_{\tilde{e},t} \dot{E}^{\text{buy,ES}}_{\tilde{e},t} - c^{\text{sell}}_{\tilde{e},t} \dot{E}^{\text{sell,ES}}_{\tilde{e},t} \right) \tag{6a}$$

s.t.

$$\sum_{k\in\mathcal{K}} \left(\dot{E}^{\text{out,ES}}_{k,e,t} - \dot{E}^{\text{in,ES}}_{k,e,t} \right) + \dot{E}^{\text{buy,ES}}_{e,t} - \dot{E}^{\text{sell,ES}}_{e,t} = \dot{E}^{\text{D}}_{e,t} \qquad \forall e \in \mathcal{E}, t \in \mathcal{T}, \tag{6b}$$

$$\boldsymbol{g}(\dot{\boldsymbol{E}}^{\text{in,ES}}_k, \dot{\boldsymbol{E}}^{\text{out,ES}}_k, \boldsymbol{x}^{\text{ES}}) \le 0 \qquad \forall k \in \mathcal{K}\backslash\mathcal{K}^{\text{PS}}, \tag{6c}$$

$$\boldsymbol{g}^{\text{ES}}_k(\dot{\boldsymbol{E}}^{\text{in,ES}}_k, \dot{\boldsymbol{E}}^{\text{out,ES}}_k, \boldsymbol{x}^{\text{ES}}) \le 0 \qquad \forall k \in \mathcal{K}^{\text{PS}}, \tag{6d}$$

$$\dot{E}^{\text{buy,ES}}_{e,t}, \dot{E}^{\text{sell,ES}}_{e,t}, \dot{E}^{\text{in,ES}}_{k,e,t}, \dot{E}^{\text{out,ES}}_{k,e,t} \in \mathbb{R}^+ \qquad \forall k \in \mathcal{K}, e \in \mathcal{E}, t \in \mathcal{T}, \tag{6e}$$

$$\boldsymbol{x}^{\text{ES}} \in \mathbb{R}^{N_{\boldsymbol{x}^{\text{ES}}}}. \tag{6f}$$

The formulation of the optimization problem at the energy system level (Problem (6)) is analogous to the original optimization problem (Problem (1)), with the following modifications: For $k \in \mathcal{K}^{\text{PS}}$, the detailed process models are replaced by their corresponding surrogate models, as shown in Eqs. (6c) and (6d). Specifically, Eq. (6d) provides a compact representation of Eqs. (2) to (5). In this formulation, $\dot{\boldsymbol{E}}^{\text{in,ES}}_{k,t}$ and $\dot{\boldsymbol{E}}^{\text{out,ES}}_{k,t}$ correspond to the decision variables $\bar{x}_t$ and $\bar{y}_t$, respectively, for each component k. Accordingly, the vector $\boldsymbol{d}^{\text{PS}}_{k,t}$ that expresses all decision variables of component k in its detailed process model can be omitted, as these decision variables are not included in the surrogate models. Furthermore, all decision variables are assigned the superscript ES to indicate their association with the simplified energy system model.

The detailed process model of each energy system component k ($k \in \mathcal{K}^{\text{PS}}$) is considered in a separate optimization problem at the process system level (denoted by the superscript PS), as presented in Eq. (7b) in Problem (7).

$$\min_{\dot{\boldsymbol{E}}^{\text{buy,PS}}_k, \dot{\boldsymbol{E}}^{\text{in,PS}}_k, \dot{\boldsymbol{E}}^{\text{out,PS}}_k, \boldsymbol{d}^{\text{PS}}_k} C^{\text{PS}}_k = \sum_{t\in\mathcal{T}} \Delta t_t \sum_{\tilde{e}\in\mathcal{E}^{\text{ext}}_k} \left(c^{\text{buy}}_{\tilde{e},t} \dot{E}^{\text{buy,PS}}_{k,\tilde{e},t} \right) \tag{7a}$$

s.t.

$$\boldsymbol{g}^{\text{PS}}_k(\dot{\boldsymbol{E}}^{\text{buy,PS}}_k, \dot{\boldsymbol{E}}^{\text{in,PS}}_k, \dot{\boldsymbol{E}}^{\text{out,PS}}_k, \boldsymbol{d}^{\text{PS}}_k) \le 0, \tag{7b}$$

$$\boldsymbol{d}^{\text{PS}}_{k,t} \in \mathcal{D}_k \subset \mathbb{R}^{N_{\boldsymbol{d}^{\text{PS}}_k}} \qquad \forall t \in \mathcal{T}, \tag{7c}$$

where the decision variables $\boldsymbol{d}^{\text{PS}}_{k,t}$ are addressed.

For clarity, we summarize the key differences between Problem (6) at the energy system level and Problem (7) at the process system level in Table 3.

Table 3
Key differences between Problem (6) and Problem (7) for component $k \in \mathcal{K}^{\text{PS}}$.

	Problem (6)	Problem (7) for k
Objective (Eq. (6a) vs. Eq. (7a))	minimize total operational cost of the entire energy system	minimize operational cost of component k
Key constraints (Eq. (6d) vs. Eq. (7b))	input-output surrogate models (linear or quadratic)	detailed process models: thermophysical properties, electrochemistry, mass and heat transfer, reaction kinetics, etc.
Key decision variables (Eqs. (6e) and (6f) vs. Eq. (7c))	input and output product flows, on/off state of k	internal process variables of k, e.g., temperature, pressure, reaction rates
Problem class	MIQCQP, MILP	MINLP, NLP, black box, etc.

3.2. Part B: operational optimization

In Part B, we solve the resulting operational optimization problem. Instead of directly addressing Problem (1), we decompose it into Problem (6) at the energy system level and multiple Problems (7) at the process system level, as illustrated in Fig. 4. Problem (6) and Problems (7) exchange information in the form of all product input and output flows, denoted by $\dot{\boldsymbol{E}}^{\text{in\&out,ES}}_{k,t,i}$ and $\dot{\boldsymbol{E}}^{\text{in\&out,PS}}_{k,t,i}$. We additionally introduce the subscript i to represent the iteration index.

As indicated in Table 4, our previous work [31] addressed the instance of a single continuous process system, while this work focuses on applications where multiple process systems coexist. With a single process system, the proposed solution approach iteratively solves Problem (6) and Problem (7) until they converge to a feasible operational strategy. To drive their convergence, the constraint $\dot{\boldsymbol{E}}^{\text{in\&out,PS}}_{k,t,i} = \dot{\boldsymbol{E}}^{\text{in\&out,ES}}_{k,t,i}$ is imposed in Problem (7) at the process system level, while a penalty term for the deviation from this constraint ($\left\| \dot{\boldsymbol{E}}^{\text{in\&out,ES}}_{k,t,i} - \dot{\boldsymbol{E}}^{\text{in\&out,PS}}_{k,t,i-1} \right\|_2^2$) is incorporated into the objective function of Problem (6) at the energy system level. Here, $\dot{\boldsymbol{E}}^{\text{in\&out,ES}}_{k,t,i}$ in the constraint and $\dot{\boldsymbol{E}}^{\text{in\&out,PS}}_{k,t,i-1}$ in the penalty term consist solely of parameters (numerical values) that are updated in each iteration (cf. Fig. 4).

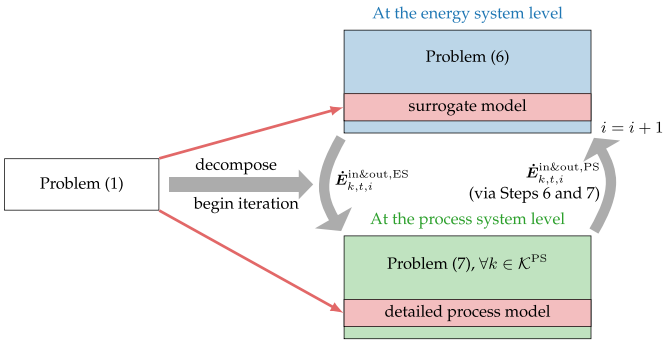

Fig. 4. Graphical illustration of the operational optimization problem addressed in Part B.

To handle the instance involving multiple process systems, this work develops three solution approaches: simultaneous, sequential and hybrid. We first present the core concept behind each solution approach (cf. the right columns in Table 4), followed by detailed explanations and implementation specifics. Note that, unless stated otherwise, the detailed update rules between the energy and process system levels within each iteration are identical to those for the instance of a single continuous process system, as presented in our previous work [31]. For the readers' convenience, an overview of these update rules is provided in the Supporting Information.

The simultaneous approach is similar to that used for the instance of a single continuous process system. However, instead of solving only one Problem (7) at the process system level, multiple such optimization problems, each corresponding to a different process system, are solved concurrently within each iteration. In contrast, the sequential approach addresses one process system at a time, solving Problem (7) for each in a predefined sequence. This sequence is determined based on the backward material flow within the energy system and is crucial for ensuring the feasibility of the decomposed optimization problems. Once a process system converges, its feasible operational decisions are obtained. We then proceed to the next process system. With the operational decisions of the previously solved process system(s) now known, we update the energy system optimization problem by replacing the corresponding surrogate models (cf. Eq. (6d)) with these fixed decisions. This update reduces the complexity of Problem (6) at the energy system level when handling the remaining process systems. The algorithm continues until all process systems are addressed. Finally, the hybrid approach is a combination of the first two approaches, allowing some process systems to be addressed simultaneously while others are handled sequentially.

The three solution approaches are designed to enhance the adaptability of our method across diverse applications. The simultaneous approach seeks to find the closest optimal operational strategy by considering all detailed process models simultaneously, but it can be computationally expensive as $\mathcal{K}^{\text{PS}}$ grows. The sequential approach prioritizes computational efficiency, aiming to quickly obtain a near-optimal feasible solution. The hybrid approach strikes a balance between solution quality and computational cost. For instance, this approach could be particularly beneficial for systems with processes that operate in parallel.

Algorithm 1 presents the detailed pseudocode implementation for solving the operational optimization problem (Part B). This implementation covers all solution approaches listed in Table 4.

To begin with, we specify input parameters for the algorithm of Part B. These include the list of energy system components with detailed process models $\mathbf{K}^{\text{PS}}$, the solution approach "whichApproach", along with the input time series, such as energy prices $c^{\text{buy\&sell}}$ and energy demands $\dot{E}^{\text{D}}$ (line 1). The list $\mathbf{K}^{\text{PS}}$ specifies the processes considered simultaneously at the process system level, depending on the chosen solution approach:

$$\text{simultaneous: } \mathbf{K}^{\text{PS}} = \Big[\big[\text{process } 1, \text{process } 2, \dots, \text{process } k\big]\Big], \tag{8a}$$

$$\text{sequential: } \mathbf{K}^{\text{PS}} = \Big[\text{process } 1, \text{process } 2, \dots, \text{process } k\Big], \tag{8b}$$

$$\text{hybrid: } \mathbf{K}^{\text{PS}} = \Big[\big[\text{process } 1, \text{process } 2\big], \dots, \text{process } k\Big]. \tag{8c}$$

The sets $\mathcal{K}^{\text{PS}}_{\text{current}}$ and $\mathcal{K}^{\text{PS}}_{\text{exclude}}$, along with the Boolean parameter "activeSequential", are defined to control which energy system components are processed and excluded, respectively, in the current sequence (lines 2 to 4). Then, the last element in $\mathbf{K}^{\text{PS}}$, denoted by $\mathbf{K}^{\text{PS}}[-1]$, is assigned to the set of current components $\mathcal{K}^{\text{PS}}_{\text{current}}$ (lines 6 to 7). The `pop()` function indicates that the corresponding element(s) are removed from $\mathbf{K}^{\text{PS}}$. As a result, when handling a single process system or multiple process systems using the simultaneous approach, $\mathbf{K}^{\text{PS}}$ is emptied directly.

Next, an empty set $\mathcal{T}^{\text{pen}}_k$ is initialized for each energy system component k in the current sequence, i.e., $k \in \mathcal{K}^{\text{PS}}_{\text{current}}$ (line 9). $\mathcal{T}^{\text{pen}}_k$ is applied to collect the time steps, where the operational decisions of k fail to converge, and this is explained later in detail in this section. Subsequently, we define the optimization problem at the energy system level (Problem (6)), taking into account the excluded energy system components $k \in \mathcal{K}^{\text{PS}}_{\text{exclude}}$ (line 11). At this point, $\mathcal{K}^{\text{PS}}_{\text{exclude}}$ is an empty set.

During the first iteration ($i = 1$), we directly solve Problem (6) to obtain the initial optimal operational decisions, including the product input and output flows $\dot{E}^{\text{in\&out,ES}}_{k,i}$ (lines 13 to 15). $\dot{E}^{\text{in\&out,ES}}_{k,i}$, $\mathcal{K}^{\text{PS}}_{\text{current}}$, $c^{\text{buy\&sell}}$, and other input parameters are then passed to the process system level, where we verify whether the operational decisions made at

Table 4
All instances of having complex process systems in an energy system. The instance with a single continuous process system is addressed in Wang et al. [31]. This work extends the method to handle multiple process systems by developing three solution approaches: simultaneous, sequential and hybrid.

single process system	multiple process systems		
	simultaneous approach	sequential approach	hybrid approach
energy system optimization process system optimization process	energy system optimization process system optimization process 1 process 2 … process k	energy system optimization process system optimization process 1 process 2 … process k	energy system optimization process system optimization process 1 process 2 … process k
previous work	this work		

Algorithm 1 Pseudocode for the algorithm of Part B, with Step 4 embedded.

procedure OPERATIONALOPTIMIZATION($\mathbf{K}^{\mathrm{PS}}$, whichApproach, $\boldsymbol{c}^{\mathrm{buy\&sell}}$, $\dot{\boldsymbol{E}}^{\mathrm{D}}$, $\mathcal{T}$)
  $\mathcal{K}^{\mathrm{PS}}_{\mathrm{current}} = []$
  $\mathcal{K}^{\mathrm{PS}}_{\mathrm{exclude}} = []$
  activeSequential = `True`

  while activeSequential **do**
    $\mathcal{K}^{\mathrm{PS}}_{\mathrm{current}} \leftarrow \mathrm{pop}(\mathbf{K}^{\mathrm{PS}}[-1])$

    $\mathcal{T}^{\mathrm{pen}}_{k} = [], \forall k \in \mathcal{K}^{\mathrm{PS}}_{\mathrm{current}}$

    define Problem (6) with $\mathcal{K}^{\mathrm{PS}}_{\mathrm{exclude}}$

    $i = 1$
    $f(\boldsymbol{x}) = C^{\mathrm{ES}}_{i}$
    $\dot{\boldsymbol{E}}^{\mathrm{in\&out,ES}}_{k,i}, \forall k \in \mathcal{K} \leftarrow$ **solve** Problem (6) by minimizing the objective function $f(\boldsymbol{x})$

    $\dot{\boldsymbol{E}}^{\mathrm{in\&out,PS}}_{k,i}, C^{\mathrm{PS}}_{k,i}, \mathcal{T}^{\mathrm{pen}}_{k}, \forall k \in \mathcal{K}^{\mathrm{PS}}_{\mathrm{current}} \leftarrow$STEP5-INTEGRATEDPROCESSSYSTEM
      OPTIMIZATION($\dot{\boldsymbol{E}}^{\mathrm{in\&out,ES}}_{k,i}$, $\mathcal{K}^{\mathrm{PS}}_{\mathrm{current}}$, $\boldsymbol{c}^{\mathrm{buy\&sell}}$, $\mathcal{T}$, $\mathcal{T}^{\mathrm{pen}}_{k}$)

    if requireEstimation == `True` **then**
      $i = 2$
      $C^{\mathrm{est,PS}}_{k,i}, \forall k \in \mathcal{K}^{\mathrm{PS}}_{\mathrm{current}} \leftarrow$STEP6-ESTIMATIONTERM
        ($\dot{\boldsymbol{E}}^{\mathrm{out,PS}}_{k,i-1}$, $\mathcal{K}^{\mathrm{PS}}_{\mathrm{current}}$, $\boldsymbol{c}^{\mathrm{buy\&sell}}$, $\mathcal{DS}_{k,e}$, $\mathcal{T}$)

      $f(\boldsymbol{x}) = C^{\mathrm{ES}}_{i} + C^{\mathrm{est,PS}}_{i}$
      $\dot{\boldsymbol{E}}^{\mathrm{in\&out,ES}}_{k,i}, \forall k \in \mathcal{K} \leftarrow$**solve** Problem (6) by minimizing the objective function $f(\boldsymbol{x})$

      $\dot{\boldsymbol{E}}^{\mathrm{in\&out,PS}}_{k,i}, C^{\mathrm{PS}}_{k,i}, \mathcal{T}^{\mathrm{pen}}_{k}, \forall k \in \mathcal{K}^{\mathrm{PS}}_{\mathrm{current}} \leftarrow$STEP5-INTEGRATEDPROCESSSYSTEM
        OPTIMIZATION($\dot{\boldsymbol{E}}^{\mathrm{in\&out,ES}}_{k,i}$, $\mathcal{K}^{\mathrm{PS}}_{\mathrm{current}}$, $\boldsymbol{c}^{\mathrm{buy\&sell}}$, $\mathcal{T}$, $\mathcal{T}^{\mathrm{pen}}_{k}$)
    end if
    repeat
      $i = i + 1$

      if requireEstimation == `True` **then**
        $C^{\mathrm{est,PS}}_{k,i}, \forall k \in \mathcal{K}^{\mathrm{PS}}_{\mathrm{current}} \leftarrow$STEP6-ESTIMATIONTERM
          ($\dot{\boldsymbol{E}}^{\mathrm{out,PS}}_{k,i-1}$, $\mathcal{K}^{\mathrm{PS}}_{\mathrm{current}}$, $\boldsymbol{c}^{\mathrm{buy\&sell}}$, $\mathcal{DS}_{k,e}$, $\mathcal{T}$)
      end if

      $C^{\mathrm{pen}}_{k,i}, \forall k \in \mathcal{K}^{\mathrm{PS}}_{\mathrm{current}} \leftarrow$STEP7-PENALTYTERM($\dot{\boldsymbol{E}}^{\mathrm{in\&out,PS}}_{k,i-1}$, $\mathcal{T}^{\mathrm{pen}}_{k}$, $\mathcal{K}^{\mathrm{PS}}_{\mathrm{current}}$)

      $f(\boldsymbol{x}) = C^{\mathrm{ES}}_{i} + C^{\mathrm{est,PS}}_{i} + C^{\mathrm{pen}}_{i}$
      $\dot{\boldsymbol{E}}^{\mathrm{in\&out,ES}}_{k,i}, \forall k \in \mathcal{K} \leftarrow$**solve** Problem (6) by minimizing the objective function $f(\boldsymbol{x})$

      $\dot{\boldsymbol{E}}^{\mathrm{in\&out,PS}}_{k,i}, C^{\mathrm{PS}}_{k,i}, \mathcal{T}^{\mathrm{pen}}_{k}, \forall k \in \mathcal{K}^{\mathrm{PS}}_{\mathrm{current}} \leftarrow$STEP5-INTEGRATEDPROCESSSYSTEM
        OPTIMIZATION($\dot{\boldsymbol{E}}^{\mathrm{in\&out,ES}}_{k,i}$, $\mathcal{K}^{\mathrm{PS}}_{\mathrm{current}}$, $\boldsymbol{c}^{\mathrm{buy\&sell}}$, $\mathcal{T}$, $\mathcal{T}^{\mathrm{pen}}_{k}$)

    until $\dot{\boldsymbol{E}}^{\mathrm{in\&out,ES}}_{k,i}$ and $\dot{\boldsymbol{E}}^{\mathrm{in\&out,PS}}_{k,i}$ converge within ϵ_k **or** $i > i^{\max}$

    if $\mathbf{K}^{\mathrm{PS}} == \emptyset$ **then** activeSequential = `False`
    end if

    if whichApproach == `sequential` **or** whichApproach == `hybrid` **then**
      $\mathcal{K}^{\mathrm{PS}}_{\mathrm{exclude}} := \mathcal{K}^{\mathrm{PS}}_{\mathrm{exclude}} \cup \mathcal{K}^{\mathrm{PS}}_{\mathrm{current}}$
    end if

  end while

  calculate total operational cost C^{total} via Eq. (12)

  return C^{total}
end procedure

the energy system level can be fulfilled by the detailed process models in Step 5 (lines 17 to 18). The actual product input and output flows at the process system level $\dot{E}^{\text{in\&out,PS}}_{k,i}$, the actual operational costs $C^{\text{PS}}_{k,i}$ and the set of penalty time steps $\mathcal{T}^{\text{pen}}_{k}$ are the outputs of Step 5. The implementation details for the integrated process system optimization (Step 5) are provided in the next subsection.

Depending on whether operational costs are included in the surrogate model of $k \in \mathcal{K}^{\text{PS}}_{\text{current}}$, an additional step (Step 6) may be required to compute estimated operational costs (line 20). The actual product output flows from the previous iteration $\dot{E}^{\text{out,PS}}_{k,i-1}$, $\mathcal{K}^{\text{PS}}_{\text{current}}$, $\boldsymbol{c}^{\text{buy\&sell}}$, the dataset $\mathcal{DS}_{k,e}$, and $\mathcal{T}$ serve as inputs for Step 6. The estimation term $C^{\text{est,PS}}_{i}$ is the sum of all estimated operational costs $C^{\text{est,PS}}_{k,i}$ and is defined as follows:

$$C^{\text{est,PS}}_{i} = \sum_{k \in \mathcal{K}^{\text{PS}}_{\text{current}}} C^{\text{est,PS}}_{k,i} = \sum_{k \in \mathcal{K}^{\text{PS}}_{\text{current}}} \sum_{t \in \mathcal{T}} f(\dot{E}^{\text{out,ES}}_{k,e,t,i}), \tag{9}$$

where $f(\dot{E}^{\text{out,ES}}_{k,e,t,i})$ generally represents a function comprising linear and quadratic expressions of decision variables $\dot{E}^{\text{out,ES}}_{k,e,t,i}$. The formulation of $f(\dot{E}^{\text{out,ES}}_{k,e,t,i})$ is based on linear interpolation of specific operational costs from the dataset $\mathcal{DS}_{k,e}$, with their gradients used as correction factors. The implementation of the estimation term (Step 6) is detailed in our previous work [31] and is applied in the same manner in this work. We then solve the updated Problem (6) at the energy system level with the revised objective function (lines 25 to 26) and subsequently Problems (7) at the process system level (lines 28 to 30).

Starting from the next iteration (lines 31 to 32), we use the results from the previous iteration to calculate the estimation term in Step 6, if necessary (lines 34 to 37), and the penalty term in Step 7 (line 39). The penalty term C^{pen}_{i} is introduced to address discrepancies in operational decisions between the energy and process system levels. To compute C^{pen}_{i}, Step 7 takes as input the actual product input and output flows from the previous iteration $\dot{E}^{\text{in\&out,PS}}_{k,i-1}$ and the set of penalty time steps $\mathcal{T}^{\text{pen}}_{k}$ for all $k \in \mathcal{K}^{\text{PS}}_{\text{current}}$. The penalty term is defined as follows:

$$\begin{aligned} C^{\text{pen}}_{i} &= \sum_{k \in \mathcal{K}^{\text{PS}}_{\text{current}}} C^{\text{pen}}_{k,i} \\ &= \sum_{k \in \mathcal{K}^{\text{PS}}_{\text{current}}} \sum_{e \in \mathcal{E}} \sum_{t \in \mathcal{T}^{\text{pen}}} \gamma_{k,e,t} \left[\left(\dot{E}^{\text{out,ES}}_{k,e,t,i} - \dot{E}^{\text{out,PS}}_{k,e,t,i-1} \right)^2 + \left(\dot{E}^{\text{in,ES}}_{k,e,t,i} - \dot{E}^{\text{in,PS}}_{k,e,t,i-1} \right)^2 \right], \end{aligned} \tag{10}$$

where $\dot{E}^{\text{in,PS}}_{k,e,t,i-1}$ and $\dot{E}^{\text{out,PS}}_{k,e,t,i-1}$ represent the results (numerical values) from iteration $i-1$, while $\dot{E}^{\text{in,ES}}_{k,e,t,i}$ and $\dot{E}^{\text{out,ES}}_{k,e,t,i}$ are decision variables for iteration i. The parameter $\gamma_{k,e,t}$ is a scaling factor associated with product e of energy system component k at time step t. $\gamma_{k,e,t}$ can either remain constant or vary depending on different k, e, and t.

After updating the objective function (line 41), the operational problem at the energy system level (line 42) and process system level (lines 44 to 45) are re-solved. This iterative procedure continues until at least one of the termination criteria is satisfied (line 47). Termination occurs when the operational decisions at the energy system level $\dot{E}^{\text{in\&out,ES}}_{k,i}$ and at the process system level $\dot{E}^{\text{in\&out,PS}}_{k,i}$ converge within a predefined tolerance ϵ_k, or when the maximum number of iterations $i^{\max}$ is reached.

As of now, the operational optimization for all energy system components in the current sequence ($k \in \mathcal{K}^{\text{PS}}_{\text{current}}$) is complete. We then examine whether any element remains in the list $\mathbf{K}^{\text{PS}}$ (lines 49 to 50). If the instance involves a single process system or multiple process systems using the simultaneous approach, the solution procedure is considered complete (cf. line 7), and we end it by updating the Boolean parameter activeSequential. If the sequential or hybrid approach is applied, the solution procedure continues until the list $\mathbf{K}^{\text{PS}}$ is emptied. Before proceeding to the next sequence, we update the set $\mathcal{K}^{\text{PS}}_{\text{exclude}}$ by adding the element(s) from $\mathcal{K}^{\text{PS}}_{\text{current}}$ (lines 52 to 54). This update indicates that the operational decisions for all $k \in \mathcal{K}^{\text{PS}}_{\text{exclude}}$ have been determined.

We then proceed with the next sequence by replacing the element(s) in $\mathcal{K}^{\text{PS}}_{\text{current}}$ with the next element from $\mathbf{K}^{\text{PS}}$ (cf. lines 6 to 7). In this way, the energy system components are addressed in the exact sequence predefined in the list $\mathbf{K}^{\text{PS}}$. With $\mathcal{K}^{\text{PS}}_{\text{exclude}}$ now non-empty, we update Problem (6) at the energy system level (cf. line 11). Since the operational decisions for all $k \in \mathcal{K}^{\text{PS}}_{\text{exclude}}$ have already been validated by the detailed process models in previous sequence(s), we replace their surrogate models with these validated operational decisions. Consequently, the constraint Eq. (6d) for $k \in \mathcal{K}^{\text{PS}}_{\text{exclude}}$ in Problem (6) are substituted with:

$$\dot{E}^{\text{in,ES}}_{k,e,t,i} = \dot{E}^{\text{in,PS}}_{k,e,t,i=i^{\text{term}}_{k}} \qquad \forall k \in \mathcal{K}^{\text{PS}}_{\text{exclude}} \subset \mathcal{K}^{\text{PS}}, e \in \mathcal{E}, t \in \mathcal{T}, \tag{11a}$$

$$\dot{E}^{\text{out,ES}}_{k,e,t,i} = \dot{E}^{\text{out,PS}}_{k,e,t,i=i^{\text{term}}_{k}} \qquad \forall k \in \mathcal{K}^{\text{PS}}_{\text{exclude}} \subset \mathcal{K}^{\text{PS}}, e \in \mathcal{E}, t \in \mathcal{T}. \tag{11b}$$

i^{term}_{k} denotes the iteration at which the iterative procedure terminates for the energy system component k when it was addressed in previous sequence(s) (cf. line 47). The order of elements in $\mathbf{K}^{\text{PS}}$, and consequently in $\mathcal{K}^{\text{PS}}_{\text{exclude}}$, determines which decision variables must be fixed when updating the optimization problem at the energy system level (Problem (6)) in subsequent sequences. Therefore, establishing an upstream ordering of energy system components based on material flows is essential to ensure the overall feasibility of the decomposed optimization problems when applying the sequential or hybrid approach.

After updating Problem (6), the subsequent iterative procedure is identical for each sequence (cf. lines 13 to 47) and continues until all elements in $\mathbf{K}^{\text{PS}}$ are addressed (cf. lines 49 to 50). Since the operational decisions provided by the detailed process models are feasible solutions, we update the total operational cost C^{total} before completing the algorithm (lines 58 to 61):

$$C^{\text{total}} = C^{\text{ES}}_{i} - \sum_{k \in \mathcal{K}^{\text{PS}}} C^{\text{ES}}_{k,i=i^{\text{term}}_{k}} + \sum_{k \in \mathcal{K}^{\text{PS}}} C^{\text{PS}}_{k,i=i^{\text{term}}_{k}}, \tag{12}$$

where C^{ES}_{i} represents the operational cost of the entire energy system during the last iteration of the final sequence at the energy system level. $C^{\text{ES}}_{k,i=i^{\text{term}}_{k}}$ and $C^{\text{PS}}_{k,i=i^{\text{term}}_{k}}$ denote the operational cost of component k ($k \in \mathcal{K}^{\text{PS}}$) at the energy and process system levels, respectively.

The algorithm identifies a feasible operational strategy for a given energy system if $\dot{E}^{\text{in\&out,ES}}_{k,i=i^{\text{term}}_{k}}$ and $\dot{E}^{\text{in\&out,PS}}_{k,i=i^{\text{term}}_{k}}$ for $k \in \mathcal{K}^{\text{PS}}$ converge within a predefined tolerance ϵ_k. This convergence condition is explained in detail in the following subsection. If the iterative procedure terminates due to reaching the maximum number of iterations ($i^{\max}$) (cf. line 47), infeasibility may occur. In the instances with a single process system or multiple process systems using the simultaneous approach, the original operational optimization problem (Problem (1)) is directly deemed infeasible. Yet, in instances applying sequential or hybrid approaches, feasible operational decisions at the process system level from the previous sequence(s) are always utilized in the optimization problems in subsequent sequence(s), regardless of the iteration in which termination occurs. Thus, only the convergence in the final sequence matters. Only if the optimization problems in the final sequence reach $i^{\max}$ and fail to converge, do we consider the original optimization problem (Problem (1)) infeasible.

In case Problem (1) is infeasible, particularly for instances with multiple process systems solved using the simultaneous approach, a sequential run could be attempted as a final effort to obtain a feasible operational strategy. Alternatively, external product purchases at higher buying prices may serve as a fallback option. However, these extensions fall outside the scope of our work and are therefore not implemented.

3.2.1. Step 5: integrated process system optimization

In Step 5, we solve the operational optimization problem at the process system level (Problem (7)). This step utilizes detailed process models and its implementation details are presented as pseudocode in Algorithm 2.

We address each energy system component k in the current sequence ($k \in \mathcal{K}^{\text{PS}}_{\text{current}}$) independently (line 4) and load the corresponding dataset

Algorithm 2 Representation of Step 5 integrated process system optimization as pseudocode.

1: **procedure** STEP5-INTEGRATEDPROCESSSYSTEM
2: OPTIMIZATION($\dot{E}_{k,i}^{\text{in\&out,ES}}$, $\mathcal{K}_{\text{current}}^{\text{PS}}$, $c^{\text{buy\&sell}}$, $\mathcal{T} = \{t_1, \dots, t_{\text{end}}\}$, $\mathcal{T}_k^{\text{pen}}$)
3:
4: **for** $k \in \mathcal{K}_{\text{current}}^{\text{PS}}$ **do**
5:
6: **load** the dataset $\mathcal{DS}_{k,e}$
7:
8: **obtain** cycle-based operational decisions N_i^{cyc}, $\mathcal{T}_i^{\text{cyc,start}}$, $\mathcal{T}_i^{\text{cyc,end}}$
9:
10: $o = 1$
11: **while** $o \le N_i^{\text{cyc}}$ **do**
12:
13: **formulate** Problem (14)
14: **solve** Problem (14)
15: $o = o + 1$
16: **end while**
17:
18: $t = t_1$
19: **while** $t \le t_{\text{end}}$ **do**
20: **if** $t \in \mathcal{T}_i^{\text{cyc,start}}$ **then**
21: conditionCycle = `True`
22: **get** o, $t_o^{\text{cyc,start}}$, $t_o^{\text{cyc,end}}$
23: **end if**
24:
25: **if** Convergence condition is not satisfied **then**
26: conditionCycle = `False`
27: **end if**
28:
29: **if** $t == t_o^{\text{cyc,end}}$ & conditionCycle == `False` **then**
30: $\mathcal{T}^{\text{pen}} \leftarrow \{t_o^{\text{cyc,start}}, \dots, t_o^{\text{cyc,end}}\}$
31: **end if**
32: $t = t + 1$
33: **end while**
34: **calculate** $C_{k,i}^{\text{PS}}$
35: **end for**
36: **return** $\dot{E}_{k,i}^{\text{in\&out,PS}}$, $C_{k,i}^{\text{PS}}$, $\mathcal{T}_k^{\text{pen}}$, $\forall k \in \mathcal{K}_{\text{current}}^{\text{PS}}$
37: **end procedure**

$\mathcal{DS}_{k,e}$, prepared earlier in Part A modeling (line 6). Problem (7) generally takes the form of a mixed-integer nonlinear program (MINLP). When directly solving Problem (7) proves challenging, as is often the case, we further decompose it into cycle-based subproblems.

We first convert the time-step-based operational decisions (indexed by subscript t) from the energy system level into cycle-based operational decisions (indexed by subscript o). This is done by determining the number of production cycles N_i^{cyc}, as well as the start and end time steps for all cycles, which are stored in sets $\mathcal{T}_i^{\text{cyc,start}}$ and $\mathcal{T}_i^{\text{cyc,end}}$, respectively (line 8). The elements within these sets follow the same order:

$$\mathcal{T}_i^{\text{cyc,start}} = \left\{ t_1^{\text{cyc,start}}, \dots, t_o^{\text{cyc,start}}, \dots, t_{N^{\text{cyc}}}^{\text{cyc,start}} \right\}, \tag{13a}$$

$$\mathcal{T}_i^{\text{cyc,end}} = \left\{ t_1^{\text{cyc,end}}, \dots, t_o^{\text{cyc,end}}, \dots, t_{N^{\text{cyc}}}^{\text{cyc,end}} \right\}. \tag{13b}$$

Given that a production cycle of current component k consists of $|S|$ segments, $t_o^{\text{cyc,end}}$ equals $t_o^{\text{cyc,start}} + |S| - 1$. In the simplest case, where current component k is a continuous process operating at steady state (i.e., $|S| = 1$), the elements in $\mathcal{T}_i^{\text{cyc,start}}$ and $\mathcal{T}_i^{\text{cyc,end}}$ are identical. Accordingly, we decompose Problem (7) into N_i^{cyc} subproblems, each defined as:

$$\min_{\dot{E}_{k,i}^{\text{buy,PS}}, \dot{E}_{k,i}^{\text{in,PS}}, \dot{E}_{k,i}^{\text{out,PS}}, \boldsymbol{d}_{k,i}^{\text{PS}}} C_{k,o,i}^{\text{PS}} = \sum_{t=t_o^{\text{cyc,start}} \in \mathcal{T}_i^{\text{cyc,start}}}^{t=t_o^{\text{cyc,end}} \in \mathcal{T}_i^{\text{cyc,end}}} \Delta t_t \sum_{\tilde{e} \in \mathcal{E}_k^{\text{ext}}} \left(c_{\tilde{e},t}^{\text{buy}} \dot{E}_{k,\tilde{e},t,i}^{\text{buy,PS}} \right) \tag{14a}$$

s.t.

$$\dot{E}_{k,e,t,i}^{\text{in,PS}} = \dot{E}_{k,e,t,i}^{\text{in,ES}} \qquad \forall e \in \mathcal{E}, t \in \left\{ t_o^{\text{cyc,start}}, \dots, t_o^{\text{cyc,end}} \right\}, \tag{14b}$$

$$\dot{E}_{k,e,t,i}^{\text{out,PS}} = \dot{E}_{k,e,t,i}^{\text{out,ES}} \qquad \forall e \in \mathcal{E}, t \in \left\{ t_o^{\text{cyc,start}}, \dots, t_o^{\text{cyc,end}} \right\}, \tag{14c}$$

$$\boldsymbol{g}_{k,i}^{\text{PS}}(\dot{\boldsymbol{E}}_{k,i}^{\text{buy,PS}}, \dot{\boldsymbol{E}}_{k,i}^{\text{in,PS}}, \dot{\boldsymbol{E}}_{k,i}^{\text{out,PS}}, \boldsymbol{d}_{k,i}^{\text{PS}}) \le 0, \tag{14d}$$

$$\boldsymbol{d}_{k,t,i}^{\text{PS}} \in \boldsymbol{\mathcal{D}}_k \subset \mathbb{R}^{N_{\boldsymbol{d}_k^{\text{PS}}}} \qquad \forall t \in \left\{ t_o^{\text{cyc,start}}, \dots, t_o^{\text{cyc,end}} \right\}. \tag{14e}$$

Problem (14) is solved for each cycle (lines 10 to 16). Ramping constraints can be incorporated if necessary, with implementation details provided in our previous work [31]. Additionally, the dataset $\mathcal{DS}_{k,e}$ can be used here to provide improved initial values for the decision variables.

After solving all Problems (14), we examine the convergence of the decomposed optimization problems by applying a Boolean parameter "conditionCycle" (lines 18 to 23). If any product input or output flow within a cycle fails to satisfy the convergence condition (lines 25 to 27), the operational decisions for the entire cycle are deemed infeasible. The corresponding time steps are then stored in the set $\mathcal{T}^{\text{pen}}$ (lines 29 to 31). The convergence condition at time step t is defined as follows:

$$\left| \frac{\dot{E}_{k,e,t,i}^{\text{in\&out,PS}} - \dot{E}_{k,e,t,i}^{\text{in\&out,ES}}}{\sum_{\tilde{t}=t_o^{\text{cyc,start}}}^{\tilde{t}=t_o^{\text{cyc,end}}} \dot{E}_{k,e,\tilde{t},i}^{\text{in\&out,PS}}} \right| \le \epsilon_k \qquad \forall e \in \mathcal{E}. \tag{15}$$

The convergence tolerance ϵ_k is freely adjustable, and its value reflects the quality of the surrogate model for each $k \in \mathcal{K}_{\text{current}}^{\text{PS}}$. After evaluating all k (lines 34 to 35), the final results are returned to Algorithm 1 for further processing (lines 36 to 37).

Note that in Problem (14) at the process system level, the objective function Eq. (14a) applies when the operational costs for component $k \in \mathcal{K}_{\text{current}}^{\text{PS}}$ are not included in its surrogate model. Otherwise, the objective function must be modified accordingly to ensure convergence. Additionally, constraints Eqs. (14b) and (14c) may be difficult or impossible to implement when a component k employs a black-box process model. In such cases, the constraints Eqs. (14b) and (14c) can be reformulated as relative error expressions and integrated into the objective function.

Furthermore, if directly solving Problem (14) remains computationally challenging, different strategies can be applied. For instance, heuristic optimization methods such as genetic algorithms can be applied, or a shortcut search path can be used to identify near-optimal solutions within the dataset $\mathcal{DS}_{k,e}$ rather than exploring the entire solution space $\boldsymbol{\mathcal{D}}_k$.

4. Case study: optimal operation of a power-to-x energy system with heterogeneous detailed process systems

4.1. Setup of the case study

In the following, we apply the decomposition method to optimize the daily operation of a real-world adapted power-to-X energy system. The entire energy system is illustrated in Fig. 5.

Energy system level

As shown in the middle part in Fig. 5, the power-to-X energy system consists of photovoltaic panels (PVs); power-to-X technologies, including a proton exchange membrane (PEM) electrolyzer, a direct air capture (DAC) plant, two identical methanation processes (MPs), and three gas tanks for H_2, CO_2 and CH_4; two traditional energy conversion components (a boiler and a combined heat and power system (CHP)); and two additional energy storage components (a battery and a thermal storage).

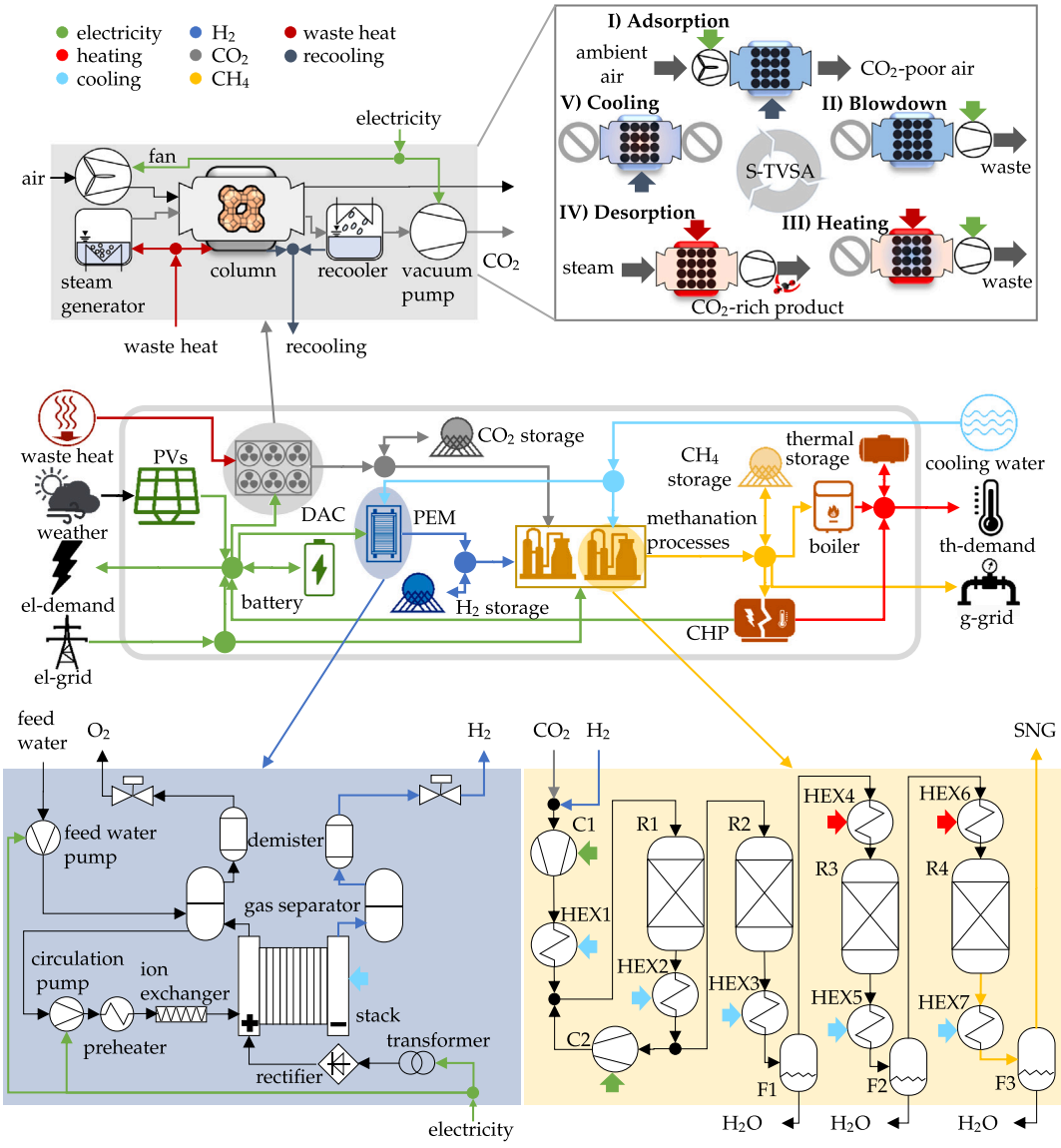

Fig. 5. Structure of the power-to-X energy system, including the detailed process models of a proton exchange membrane (PEM) electrolyzer, an adsorption-based direct air capture (DAC) plant and two identical methanation processes (MPs). The illustration of the energy system is adapted from Wang et al. [2]; the PEM electrolyzer is based on Buttler and Spliethoff [35]; the DAC plant is sourced from Postweiler et al. [36]; and the MPs are from Wang et al. [31]. PVs: photovoltaic panels, CHP: combined heat and power system, C: compressor, R: reactor, HEX: heat exchanger, F: flash, SNG: synthetic natural gas, el: electricity, g: natural gas, th: heating, and S-TVSA: steam-assisted temperature vacuum swing adsorption.

The energy system should be operated with minimal operational cost while fulfilling the electricity (el-) and heating (th-) demands at every time step. A total of seven product flows are involved: electricity, H_2, CO_2, CH_4, heating, cooling and waste heat ($\mathcal{E} = \{\text{el}, H_2, CO_2, CH_4, \text{th}, \text{co}, \text{wh}\}$). External energy supplies include the el-grid and renewable electricity from PVs which depend on weather conditions. Additionally, waste heat and cooling water supplies are assumed to be available at certain buying prices. The waste heat is exclusively used for the DAC plant, while the cooling water serves the PEM electrolyzer and MPs. Furthermore, the el-grid provides a direct electricity supply to the MPs. Any surplus CH_4 can be fed into the natural gas (g-) grid. The input time series, provided at an hourly resolution, is available in the Supporting Information.

We model each energy system component based on its input–output relationships. Their mathematical formulations, which include both linear and quadratic terms, are given in the Supporting Information and in our Git repository [37]. Here, Problem (6) at the energy system level is formulated as a mixed-integer quadratically constrained quadratic programming (MIQCQP) problem.

Process system level

Four detailed process models are applied: one for the PEM electrolyzer, one for the DAC plant, and two for the identical MPs. We treat the PEM electrolyzer and the two MPs as continuous process systems, without and with ramping constraints, respectively, and the DAC plant as a multistage batch process system.

Proton exchange membrane electrolyzer. The basic layout of a PEM electrolyzer, adapted from Buttler and Spliethoff [35], is shown on the bottom left of Fig. 5. After pretreatment, such as initial heating during start-up and deionization, feed water is brought to the electrolysis stack. The electrolysis stack consists of multiple cells built on bipolar plates assembled in series. In each cell, the electrolysis process is driven by DC electricity, producing O_2 at the anode and H_2 at the cathode. Both O_2

Table 5
Overview of parameters and boundary values for decision variables in the detailed process model of the DAC plant.

Symbol	Description	Value/Boundary	Unit
parameter			
$\tau_{\text{adsorption}}$	time duration of the adsorption phase	10346.4	s
τ_{blowdown}	time duration of the blowdown phase	30	s
τ_{heating}	time duration of the heating phase	64.6	s
$\tau_{\text{desorption}}$	time duration of the desorption phase	13043.6	s
decision variable			
τ_{cooling}	time duration of the cooing phase	$[0, \infty]$[a]	s
$\dot{m}_{\text{ads}}$	mass flow rate of air during the adsorption phase	$[1 \times 10^{-5}, 2 \times 10^{-4}]$	kg/s
p_{des}	operational pressure during the desorption phase	[0.01, 0.3]	bar
T_{des}	operational temperature during the desorption phase	[80, 100]	°C
$\dot{m}_{\text{ste}}$	mass flow rate of the steam during the desorption phase	$[1 \times 10^{-9}, 1 \times 10^{-7}]$	kg/s

[a] Although τ_{cooling} has an infinite upper bound, the results remain within a time duration range that does not affect the resulting number of segments in the surrogate model.

and H_2 pass through post-treatment, e.g., a dry demister, before being collected in a gas tank (O_2) or fed into the downstream process (H_2). This work neglects the downstream processing and use of the by-product O_2.

Generally, the cold and warm start-up times of a PEM electrolyzer are approximately 5 to 10 minutes and less than 10 seconds, respectively [35]. Compared to the hourly resolution utilized at the energy system level, we treat the PEM electrolyzer as a continuous process system, assuming that ramping constraints between adjacent time steps are negligible.

The detailed process model of the PEM electrolyzer is based on the previous work by Anand et al. [38], which builds on Gabrielli et al. [15]. The model captures electrochemical reactions, mass and heat transfer phenomena, and relevant physical properties, and incorporates several nonlinear formulations. We scale the number of cells to linearly increase the nominal size of the PEM electrolyzer for our case study application. The selected decision variables of the detailed process model ($\boldsymbol{d}^{\text{PS}}_{\text{PEM}}$) are provided in the Supporting Information.

Direct air capture plant. An adsorption-based DAC plant with a capacity of 4 kt_{CO_2}/a, sourced from Postweiler et al. [36], is considered. The DAC plant consists of five main process units (a fan, a steam generator, an adsorption/desorption column, a recooler/condenser, and a vacuum pump), as shown in the upper left of Fig. 5, and operates through a steam-assisted temperature vacuum swing adsorption (S-TVSA) cycle that progresses through five phases (adsorption, blowdown, heating, desorption, and cooling), as illustrated in the upper right part of Fig. 5.

In the adsorption phase, the fan draws ambient air through the column, where CO_2 and H_2O are captured. Next, during the blowdown phase, the column inlet is closed, and the vacuum pump reduces the column pressure to the desorption level. Then, in the heating phase, a jacket heats the column to the required desorption temperature. Once the operational temperature and pressure inside the column are ready, the DAC plant enters the desorption phase, where superheated steam is injected to release CO_2 from the column. Finally, in the cooling phase, the column is cooled to below 90 °C to prepare for the next production cycle. Upon completion, the DAC plant is ready to begin the cycle anew.

The detailed process model of the DAC plant was developed by Postweiler et al. [36] using the programming language Modelica. The model includes detailed representations of mass and heat transfer as well as adsorption equilibrium and is formulated as a system of differential-algebraic equations (DAE). This work treats this DAE system as a black-box model. The parameter values and the operational decision variables ($\mathbf{d}^{\text{PS}}_{\text{DAC}}$) are listed in Table 5. We fix the time durations for the adsorption, blowdown, heating and desorption phases, based on reference values provided in the literature [36], while the time duration of the cooling phase is treated as a decision variable. The cooling phase ends once the average adsorbent temperature drops below 90 °C. In the detailed process model, the cooling demand during the cooling phase is associated with mechanical work and converted into electricity consumption using a constant correlation factor.

Additionally, ambient conditions, particularly air humidity, also influence the operational performance of the DAC plant [36,39]. Our work utilizes the same data as in Postweiler et al. [36], though these data can be readily integrated as input parameters with an updated black-box model as needed.

Methanation processes. The energy system includes two identical Topsøe Recycle Energy-efficient Methanation Processes (TREMP™) that can operate in parallel. The flowsheet for the two MPs is shown on the lower right part of Fig. 5. Their detailed process models are adopted from our previous work [31] and include physical properties as well as catalytic chemical reactions, resulting in high nonlinearities and nonconvexities. The process description, the relevant decision variables ($\boldsymbol{d}^{\text{PS}}_{\text{MPs}}$), and their boundary values are provided in the Supporting Information.

4.2. Implementation and solution details

The decomposition method is implemented in Python 3.8 using the following packages: COMANDO [40] for the energy system modeling; GEKKO [41] and IDAES [42] for the process system modeling of the PEM electrolyzer and MPs, respectively. The dynamic model of the DAC plant is available as a functional mock-up unit [43].

The resulting non-convex MIQCQP problem at the energy system level is solved using the commercial solver Gurobi 11.0.2 [44] with an optimality gap of 5×10^{-4}. At the process system level, the resulting NLP problems for the PEM electrolyzer and MPs are solved via the open-source solver Ipopt [45] with a convergence tolerance of 1×10^{-4}. The dynamic optimization problem for the DAC plant is solved using a particle swarm optimization (PSO) algorithm [46] in the modeling part (Part A), and through a shortcut search path in the operational optimization part (Part B). In principle, applying Ipopt to the DAC model would be possible if the DAE were reformulated into algebraic constraints. Nevertheless, the choice of model formulation and solver does not compromise the effectiveness of the proposed method. The convergence criteria used in Part B are defined as follows: $\epsilon_{\text{PEM}} = 2.2 \times 10^{-2}$, $\epsilon_{\text{DAC}} = 3 \times 10^{-2}$, and $\epsilon_{\text{MP}} = 2 \times 10^{-2}$. All computations are performed on Intel® Xeon® W-2155 processors with 3.3GHz and 128GB RAM. Additional details can be found in our Git repository [37].

4.3. Part A results: surrogate modeling of a multistage process system

This subsection presents the results for Part A modeling, focusing on the DAC plant as a complex multistage batch process system. The Part A results for the PEM electrolyzer are available in the Supporting Information, and those for the MPs are available in our previous work [31].

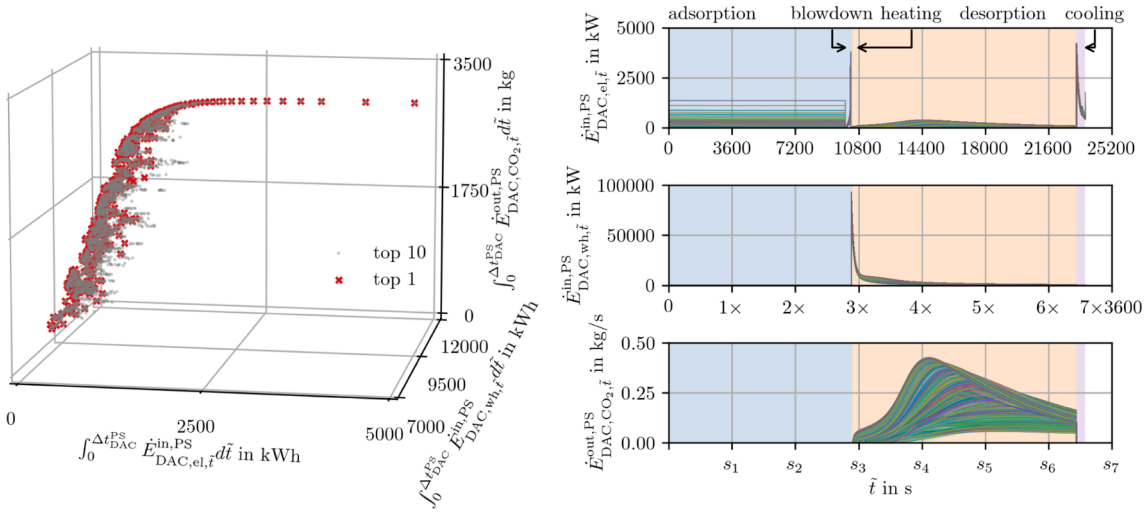

(a) Total (b) Differential

Fig. 6. Input–output relationships for all $v_{\mathrm{DAC,CO_2}} \in \mathcal{V}_{\mathrm{DAC,CO_2}}$ of the DAC plant. Left: Total input and output product amounts over a complete cycle, with the best solutions (red crosses) and the next nine best solutions (grey circles) obtained by the PSO algorithm (x-axis: electricity input, y-axis: waste heat input, and z-axis: CO_2 output). Right: Time profiles of the differential input–output states, with the five phases distinguished by different background colors (top: electricity input, middle: waste heat input, bottom: CO_2 output). A complete production cycle of the DAC plant takes approximately 6 hours and 30 minutes. To match the hourly resolution of the energy system model, the production cycle is decomposed into seven segments, i.e., $\mathcal{S} = \{s_1, s_2, s_3, s_4, s_5, s_6, s_7\}$.

The electricity and waste heat serve as the external energy supply for operating the stand-alone DAC plant to obtain the output product CO_2, i.e., $\mathcal{E} = \{\mathrm{el}, \mathrm{wh}, \mathrm{CO_2}\}$. The buying prices of the external electricity and waste heat supplies in Part A are fixed at 0.2 EUR/kWh and 0.045 EUR/kWh, respectively. The optimization problem for generating the (near-)optimal operational dataset $\mathcal{DS}_{\mathrm{DAC,CO_2}}$ is defined as follows:

$$\begin{aligned}\min_{\dot{\boldsymbol{E}}^{\mathrm{buy,PS}}_{\mathrm{DAC}},\dot{\boldsymbol{E}}^{\mathrm{in,PS}}_{\mathrm{DAC}},\dot{\boldsymbol{E}}^{\mathrm{out,PS}}_{\mathrm{DAC}},\boldsymbol{d}^{\mathrm{PS}}_{\mathrm{DAC}}} \quad C^{\mathrm{PS}}_{\mathrm{DAC}} &= \int_0^{\Delta t^{\mathrm{PS}}_{\mathrm{DAC}}} c^{\mathrm{buy}}_{\mathrm{wh},\tilde{t}} \dot{E}^{\mathrm{buy,PS}}_{\mathrm{DAC,wh},\tilde{t}} \mathrm{d}\tilde{t} \\ &+ \int_0^{\Delta t^{\mathrm{PS}}_{\mathrm{DAC}}} c^{\mathrm{buy}}_{\mathrm{el},\tilde{t}} \dot{E}^{\mathrm{buy,PS}}_{\mathrm{DAC,el},\tilde{t}} \mathrm{d}\tilde{t} \\ &+ \left(\int_0^{\Delta t^{\mathrm{PS}}_{\mathrm{DAC}}} \dot{E}^{\mathrm{out,PS}}_{\mathrm{DAC,CO_2},\tilde{t}} \mathrm{d}\tilde{t} - v_{\mathrm{DAC,CO_2}} \right)^2 \end{aligned} \tag{16a}$$

s.t.

$$\boldsymbol{g}^{\mathrm{PS}}_{\mathrm{DAC}} \left(\dot{\boldsymbol{E}}^{\mathrm{buy,PS}}_{\mathrm{DAC}}, \dot{\boldsymbol{E}}^{\mathrm{in,PS}}_{\mathrm{DAC}}, \dot{\boldsymbol{E}}^{\mathrm{out,PS}}_{\mathrm{DAC}}, \boldsymbol{d}^{\mathrm{PS}}_{\mathrm{DAC}} \right) \leq 0, \tag{16b}$$

$$\boldsymbol{d}^{\mathrm{PS}}_{\mathrm{DAC}} \in \mathcal{D}_{\mathrm{DAC}} \subset \mathbb{R}^{N_{\boldsymbol{d}^{\mathrm{PS}}_{\mathrm{DAC}}}}. \tag{16c}$$

The time duration $\Delta t^{\mathrm{PS}}_{\mathrm{DAC}}$ corresponds to a full production cycle of the DAC plant. The detailed process model included in Eq. (16b) is a black-box model consisting of dynamic-algebraic equations. Therefore, we use $\tilde{t}$ to differentiate it from t due to differing time resolutions and directly incorporate the required amount of CO_2 output for a full cycle $v_{\mathrm{DAC,CO_2}}$ into the objective function (Eq. (16a)), where $v_{\mathrm{DAC,CO_2}} \in \mathcal{V}_{\mathrm{DAC,CO_2}} = \{550\,\mathrm{kg}, 555\,\mathrm{kg}, \ldots, 3000\,\mathrm{kg}\}$.

We solve Problem (16) for each element of $\mathcal{V}_{\mathrm{DAC,CO_2}}$ and compile the results into $\mathcal{DS}_{\mathrm{DAC,CO_2}}$. A total of 490 optimization runs are conducted. The parameters and the convergence performance of the PSO algorithm used are provided in the Supporting Information. The results of all optimization runs are illustrated in Fig. 6.

Fig. 6(a) presents the total electricity (x-axis) and waste heat inputs (y-axis), along with the total CO_2 output (z-axis) of a production cycle, for the best (red crosses) and next nine best (grey circles) solutions of each optimization run. Generally, as the total CO_2 output increases, the total waste heat input rises, while the total electricity input fluctuates between a minimum threshold and a higher value. When the CO_2 output approaches its limit (approximately 2977.5 kg), electricity consumption increases dramatically due to the need for higher input air flow during the adsorption phase, a lower desorption pressure level during the desorption phase, and a substantial rise in cooling demand during the cooling phase. The distribution of the decision variables listed in Table 5 as a function of the total CO_2 output is presented in the Supporting Information.

Fig. 6(b) shows the time profile of the differential input–output states of a production cycle of the column, displaying electricity input (top), waste heat input (middle), and CO_2 output (bottom). The five phases are differentiated with different background colors. The blowdown and heating phases are very brief and thus barely visible in the figures. The time duration of the cooling phase varies slightly for different CO_2 outputs, between 0 to around 200 seconds. High electricity input is observed during the cooling phase due to the correlation between cooling demand and mechanical work in the black-box model. The rise in the electricity input at the end of the cycle is attributed to the cyclic steady-state constraints applied in the black-box model, forcing the final state of the cooling phase to equal the initial state of the adsorption phase.

Given the heuristic nature of PSO algorithms, we compile the top 10 solutions (rather than just the top 1 solution) of each optimization run into $\mathcal{DS}_{\mathrm{DAC,CO_2}}$. As a result, a total of 4189 unique (near-)optimal operational data points are used to generate the surrogate model for the DAC plant.

A complete production cycle of the DAC plant takes approximately 6 hours and 30 minutes (cf. Fig. 6(b)). Given the hourly resolution at the energy system level, we decompose the entire cycle into seven segments ($\mathcal{S} = \{s_1, s_2, s_3, s_4, s_5, s_6, s_7\}$). Namely, once the DAC plant begins operation, it requires seven consecutive time steps to complete one production cycle (cf. Section 3.1). The operational data and surrogate models for four selected segments at the segment domain (cf. the second row of Table 2) are shown in Fig. 7, while the remaining three segments are provided in the Supporting Information.

Figs. 7(a–d) present the operational data (represented as gray markers) and surrogate models (depicted by colored lines) of segments s_1, s_3, s_5 and s_7, respectively. We select these four segments to highlight the significant variations in operational decisions for the DAC plant throughout a production cycle. Referring to Fig. 6(b), segment s_1 is inside the adsorption phase, where the DAC plant requires electricity to blow air into the plant, with neither waste heat input nor CO_2 output. Segment

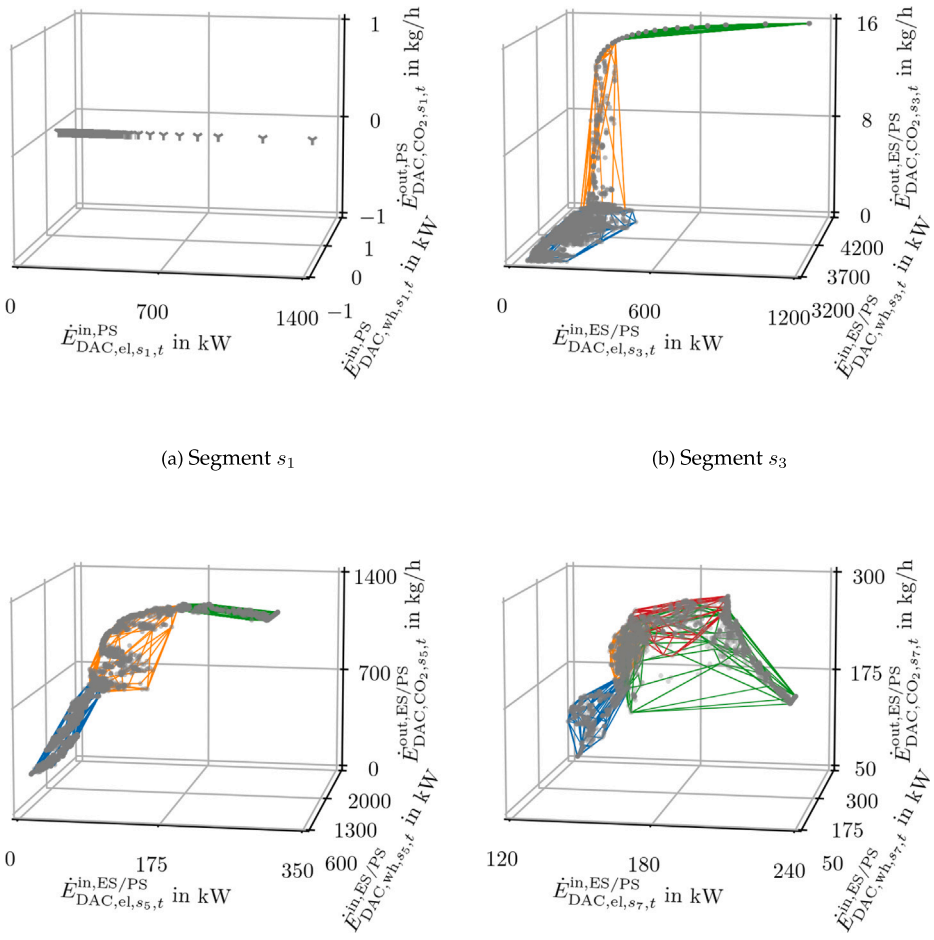

(a) Segment s_1

(b) Segment s_3

(c) Segment s_5

(d) Segment s_7

Fig. 7. Operational data and surrogate models for the DAC plant at the segment domain. Gray markers represent operational data at the process system level (PS), while the colored lines depict the corresponding convex regions, which form part of the surrogate models for the DAC plant at the energy system level (ES). Four selected segments are shown, with the axes indicating electricity input (x-axis), waste heat input (y-axis), and CO_2 output (z-axis). The convex region of segment s_1 is a straight line and thus not illustrated.

s_3 includes a partial adsorption phase, complete blowdown and heating phases, and a small partial desorption phase. Thus, most data points in the segment s_3 show very low CO_2 output (less than 0.02 kg/h), while the waste heat input spans a different order of magnitude, varying between 3200 and 4200 kW. Segment s_5 belongs to the desorption phase, while segment s_7 includes both the desorption and cooling phases.

The distribution of data points reflects not only the varying interactions of the product input and output flows across different segments but also the wide range of their values. Given the high level of nonlinearity observed, we apply the concept of convex region surrogate models [47] to approximate the feasible region for each segment (cf. the second row of Table 2). To improve precision, we manually partition the data points within each segment into three or four regions based on their distribution, as illustrated with different colored lines in Fig. 7. The corresponding number of data points per region is provided in the Supporting Information. Alternatively, an automatic splitting approach, such as the one proposed by Zhang et al. [47], can be applied, if needed.

Alongside the convex region surrogate models for each segment, we apply multivariate linear regression to model the interactions between input and output product flows across all segments within a production cycle of the DAC plant (cf. the last row of Table 2). The multivariate linear regression model is generated via the Python package `scikit-learn` [48]. All 4189 data points are split into 80:20 for model training and testing, respectively. The resulting surrogate model achieves an R^2 score of 99.6 % and is detailed as follows:

$$
\begin{aligned}
&Y = \Theta^{\intercal} X,\\
&Y = \begin{bmatrix} \dot{E}^{\text{out,ES}}_{\text{DAC,CO}_2,s_3,t} & \dot{E}^{\text{out,ES}}_{\text{DAC,CO}_2,s_4,t} & \cdots & \dot{E}^{\text{out,ES}}_{\text{DAC,CO}_2,s_7,t} \end{bmatrix},\\
&X = \begin{bmatrix} 1 & \dot{E}^{\text{in,ES}}_{\text{DAC,el},s_1,t} & \dot{E}^{\text{in,ES}}_{\text{DAC,el},s_2,t} & \cdots & \dot{E}^{\text{in,ES}}_{\text{DAC,el},s_7,t} \\ & & \dot{E}^{\text{in,ES}}_{\text{DAC,wh},s_3,t} & \dot{E}^{\text{in,ES}}_{\text{DAC,wh},s_4,t} & \cdots & \dot{E}^{\text{in,ES}}_{\text{DAC,wh},s_7,t} \end{bmatrix}.
\end{aligned}
\tag{17}
$$

A total of 17 decision variables are included in Eq. (17), representing the product input and output flows of all seven segments for the DAC plant at time step t (cf. Eq. (5a)). The values of the parameter matrix Θ are provided in the Supporting Information.

4.4. Part B results: operational optimization with multiple detailed process models

We solve the operational optimization problem for the power-to-X energy system via two methods: the decomposition method with the three proposed approaches illustrated in Table 4 and a reference method, as listed in Table 6.

First, the decomposed optimization problems are solved via the simultaneous, sequential and hybrid approaches, respectively. Instead of

Table 6
Different methods to solve the operational optimization problem.

Solution method	This work			Reference
Approach	Simultaneous	Sequential	Hybrid	–
Model description				
Detailed process models		PEM, DAC, MP1, MP2		–
Sequence	–	MP2 → MP1 → DAC → PEM	{MP1, MP2} → DAC → PEM	–
Size of		Problem (6)[a]		Problem (1)
No. of constraints	6064	6064 → 5824 → 5584 → 2758	6064 → 5584 → 2758	3533
No. of binary variables	1712	1712→ 1640 → 1568 → 846	1712 → 1568 → 846	1040
No. of continuous variables	48,253	48,253 → 48,109 → 47,965 → 1378	48,253→ 47,965 → 1378	1837
Maximum number of iterations	20	10 → 10 → 10 → 10	20 → 10 → 10	–
Scale factor	$\gamma_{\text{PEM}} = 1, \gamma_{\text{DAC,CO}_2} = 0.2$ $\gamma_{\text{DAC,wh}} = 0.05, \gamma_{\text{DAC,el}} = 0.2$ $\gamma_{\text{MP1}} = 2, \gamma_{\text{MP2}} = 2$			–

[a] In the sequential and hybrid approaches, the number following each arrow indicates the number of the remaining constraints or decision variables after fixing the operational decisions of preceding energy system component(s) (cf. line 11 in Algorithm 1).

directly solving Problem (1), we decompose it into one Problem (6) at the energy system level and four optimization problems at the process system level, i.e, one Problem (7) for each $k \in \mathcal{K}^{\text{PS}} = \{\text{PEM}, \text{DAC}, \text{MP1}, \text{MP2}\}$. Further, each Problem (7) is decomposed into subproblems, Problems (14), with up to 24 for the PEM electrolyzer, 3 for the DAC plant, and 2 × 24 for the MPs. Consequently, up to 76 decomposed optimization problems are solved in each iteration. In the simultaneous approach, all four energy system components are considered during each iteration ($\mathbf{K}^{\text{PS}} = \left[\left[\text{PEM}, \text{DAC}, \text{MP1}, \text{MP2}\right]\right]$). In the sequential approach, the energy system components are addressed in their upstream order ($\mathbf{K}^{\text{PS}} = \left[\text{PEM}, \text{DAC}, \text{MP1}, \text{MP2}\right]$, cf. line 7 in Algorithm 1). The hybrid approach first processes the MPs simultaneously, followed sequentially by the DAC plant and then the PEM electrolyzer ($\mathbf{K}^{\text{PS}} = \left[\text{PEM}, \text{DAC}, \left[\text{MP1}, \text{MP2}\right]\right]$). Additionally, we implement a reference method to address Problem (1) in a state-of-the-art manner. In this method, all energy system components are modeled with simplified constant input–output relationships across all time steps, as detailed in the Supporting Information. As clarified earlier, Problem (1) cannot be solved using state-of-the-art methods when detailed process models are included. Therefore, the reference method applies the model simplification and serves solely as a benchmark for the modeling part of the proposed method.

The optimization problem size at the energy system level varies across the solution methods. Compared to the reference method, which has the smallest problem size, our solution method includes a significantly larger number of constraints and continuous variables, mainly owing to the application of the convex region surrogate models. In the simultaneous approach, the size of Problem (6) is the largest and remains constant during the whole solution procedure. In the sequential and hybrid approaches, the size of Problem (6) decreases as surrogate models are progressively replaced by fixed values of decision variables.

We set the maximum number of iterations $i^{\max}$ for our solution approaches to 20 if $\mathcal{K}^{\text{PS}}_{\text{current}}$ contains more than one energy system element, and 10 otherwise. The scale factor $\gamma_{k,e}$ used in the penalty term is defined heuristically. For the DAC plant, three different scale factors are applied to its product input and output flows to account for their numerical differences across orders of magnitude (cf. the coordinate values in Fig. 7).

We evaluate the Part B results in terms of computational performance in Section 4.4.1. A sensitivity analysis of the scale factors on the method's performance is presented in Section 4.4.2.

4.4.1. Part B results: computational performance

A brief summary of the computational results for all solution methods is provided in Table 7. The simultaneous and sequential approaches yield nearly identical total operational costs; however, the sequential approach requires significantly more computing time—approximately 50% longer. The hybrid approach delivers the best computational results among the three proposed approaches, achieving both the shortest computing time (42 minutes) and the lowest total operational cost (29.2 EUR/d lower than the simultaneous and 24.9 EUR/d lower than the sequential). The reference method seems to provide the overall best computational results, with minimal computing time and the lowest total operational cost. However, its operational decisions are infeasible in practice, revealing that traditional simplified optimization models for addressing operational problems of such renewables-based energy systems can significantly underestimate the daily operational cost. An intuitive comparison of the resulting operational decisions from all solution methods is provided in the Supporting Information.

The computational results of the simultaneous and sequential approaches deviate slightly from our initial expectations. Therefore, in the following, we present a detailed analysis of the method's performance, focusing on computing time and resulting operational decisions.

Fig. 8 shows the distribution of computing time per iteration for our solution method. The first row illustrates the simultaneous approach (Fig. 8(a)), the second row represents the sequential approach (Figs. 8(b–e)), and the third row depicts the hybrid approach (Figs. 8(f–h)).

Table 7
Summary of the computational results for all solution methods.

Solution method	This work			Reference
Approach	Simultaneous	Sequential	Hybrid	–
Feasibility	Yes	Yes	Yes	No
Total operational cost in EUR/d	5958.7	5954.4	5929.5	5457.7
Total computing time in s	3310	5040	2536	25

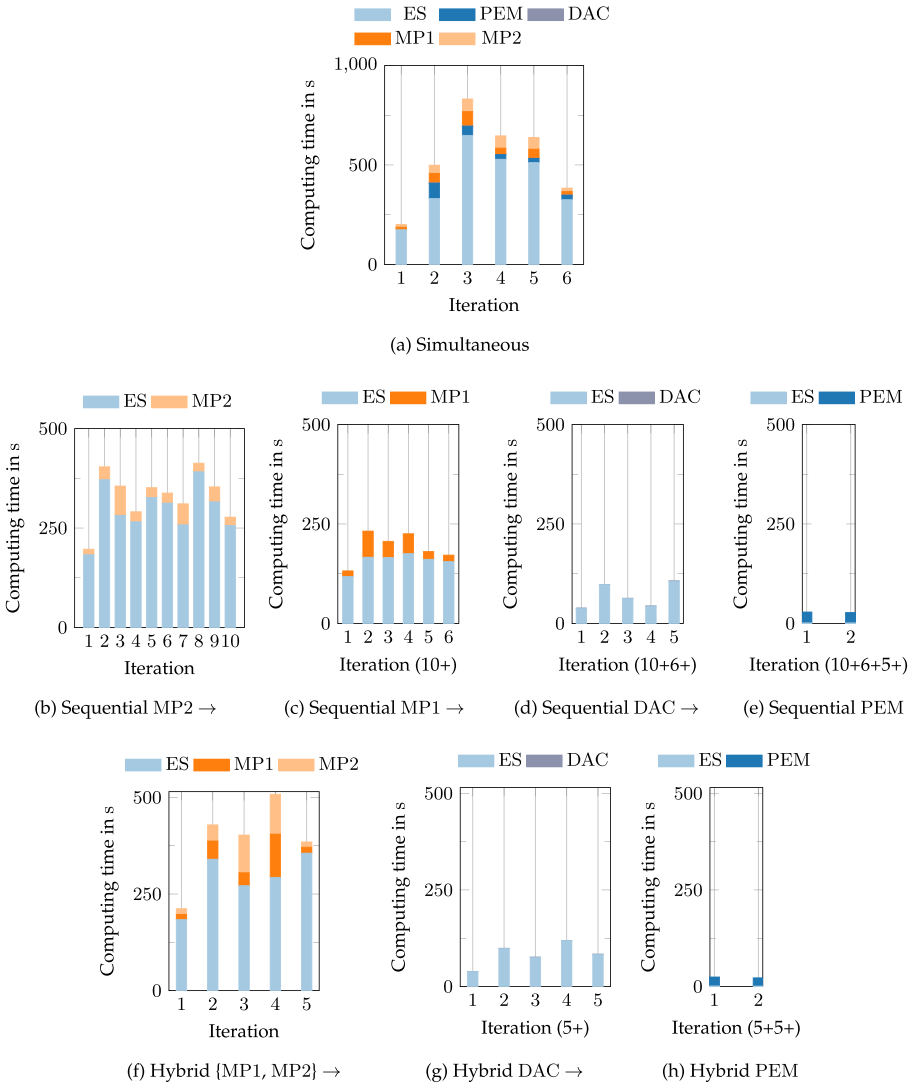

Fig. 8. Distribution of computing time per iteration for our solution method. The first, second, and third rows correspond to the simultaneous, sequential, and hybrid approaches, respectively. Different colored bars represent the computing time consumed for solving Problem (6) at the energy system level (ES) and for solving Problems (14) at the process system level.

The simultaneous approach requires only six iterations to determine the final operational decisions (cf. Fig. 8(a)). However, each iteration demands significant computing time, primarily caused by solving the optimization problems at the energy system level (Problem (6)). Here, computing time increases as the number of decision variables in the objective function grows. In the second iteration, 48 decision variables are added to the objective function because of the estimation term introduced through the MPs. From the third iteration onward, the penalty term becomes active. By the third iteration, the penalty term includes 22 decision variables, which increase to 44 by the fifth iteration. This results in an average computing time of approximately 7 minutes for solving Problem (6).

Moreover, the computing time at the process system level is significantly lower than that at the energy system level. For the PEM electrolyzer, treated as a continuous process without ramping constraints, the computing time is solely dictated by the progression of the IPOPT solver and remains below 30 seconds (except in the second iteration). The DAC plant applies a shortcut search path to identify the optimal operational decisions within the dataset $DS_{\mathrm{DAC,CO_2}}$. As a result, the computing time for the DAC plant in all iterations of all solution approaches is under 0.4 seconds, making it barely noticeable in the figures.

The computing time for the MPs varies. Longer computing time for an MP indicates a higher number of time steps where operational decisions fail to converge. In such cases, alternative operational decisions are computed at the process system level, leading to increased computing time.

The sequential approach solves the decomposed operational problems in a specific order (cf. Figs. 8(b–e)). A total of 23 iterations is required to determine the final operational decisions, with 10 iterations for the MP2, 6 for the MP1, 5 for the DAC plant, and 2 for the PEM electrolyzer.

The longest computing time of an iteration occurs when addressing the first energy system component, i.e., the MP2. As shown in Fig. 8(b), the average computing time per iteration is just under 5.5 minutes. Compared to the parallel approach, the penalty term in the sequential approach includes fewer decision variables. For example, in the third iteration, only one decision variable is penalized. From the third iteration onward, only one or two additional decision variables are added to the penalty term per iteration. By the 10th iteration, with eight decision variables penalized, the operational decisions for the MP2 finally converge. The relatively slow convergence is due to the fact that only one energy system component has been addressed so far. As the restrictions

from other process models are not yet considered, the operational decisions at the energy system level retain more flexibility, and are examined solely through the detailed process model of the MP2.

Next, the sequential approach addresses the MP1, as shown in Fig. 8(c). With the surrogate model for the MP2 replaced by its known operational decisions, the optimization problems become less complex. Therefore, fewer iterations are needed, and solving Problem (6) for each iteration takes approximately only half the computing time compared to addressing the MP2 (cf. light blue bars in Figs. 8(b) and (c)).

The sequential approach continues by addressing the next upstream energy system component, as shown in Fig. 8(d). Since no ramping constraint is applied to the DAC plant, the penalty term becomes active from the second iteration onward. In this iteration, one production cycle is penalized, adding a total of 17 decision variables to the objective function. From the third iteration onward, 2 production cycles (34 decision variables) are penalized. Despite the comparatively large number of decision variables in the penalty term, Problem (6) is still less complex than the one addressed in the simultaneous approach. Thus, the computing time is significantly shorter (taking less than 1.5 minutes).

The last upstream energy system component addressed is the PEM electrolyzer. The resulting Problem (6) is now so simple that the required computing time is less than 1.5 seconds, making it barely noticeable in Fig. 8(e).

The distribution of computing time for the hybrid approach is illustrated in Figs. 8(f–h). First, when addressing the MPs simultaneously, only five iterations are required (cf. Fig. 8(f)). The computing time at the energy system level is comparable to that of the sequential approach (cf. light blue bars in Fig. 8(b)). However, it increases significantly at the process system level. For example, in the fourth iteration, seven penalized decision variables (three from the MP1 and four from the MP2) are included in the objective function of Problem (6). This represents a notable increase in computing time over the sequential approach, where only 1 or 2 penalized decision variables are identified per iteration. Nevertheless, the hybrid approach still benefits from reduced complexity, as the DAC plant and PEM electrolyzer are not yet addressed in this sequence. Once the operational decisions for MP1 and MP2 are finalized, the hybrid approach proceeds to the upstream energy system components. The computing time for optimizing the DAC plant, as shown in Fig. 8(g), and then the PEM electrolyzer, as illustrated in Fig. 8(h), closely matches the computational performance observed in the sequential approach (cf. Figs. 8(d) and (e)).

In brief, the simultaneous approach, particularly the optimization problem at the energy system level, requires substantial computing time per iteration but needs fewer iterations to reach the final feasible operational decisions. Compared to the sequential approach, the simultaneous approach is faster overall due to the dominant effect of fewer iterations. In contrast, the sequential approach needs many more iterations, though each iteration is computationally less intensive. The hybrid approach achieves a balance between the number of iterations and the computing time per iteration, resulting in the lowest total computing time so far.

The resulting operational decisions are illustrated in Fig. 9, encompassing decisions made at both the energy (ES) and process system (PS) levels. The columns represent the different solution approaches, while the rows correspond to the MPs, the DAC plant, and the PEM electrolyzer, respectively. As we only present the final results here, the operational decisions satisfy the given convergence criterion ϵ_k (cf. Section 4.2), making the differences in product output flows between the two levels (ES and PS) barely noticeable.

The operational decisions for the MP1 and the MP2 exhibit a similar pattern in both the simultaneous (cf. Figs. 9(a) and (d)) and hybrid (cf. Figs. 9(c) and (f)) approaches, as the MPs are optimized simultaneously. Additionally, the operational costs for producing CH_4 amount to approximately 110 EUR/d and are nearly evenly shared between the two MPs. In the sequential approach, however, the operational costs of MPs are slightly higher (by 9 EUR/d), with operational costs of the MP1 (cf. Fig. 9(e)) being about 4.4 times higher than those of the MP2 (cf. Fig. 9(b)).

In the sequential approach, the MP2 is addressed before the MP1. Since operating the MP1 incurs no operational costs by then, CH_4 production is shifted to the MP1. This also explains why, for more than half of the time steps, the MP1 operates at over 90% of its full load capacity. When the MP1 is eventually addressed, operational decisions for the MP2 are already fixed, and the total amount of CH_4 produced by the MP1 is also fixed, leading to extra restrictions on its operational decisions and thus higher operational costs in total.

All three approaches identify similar operational decisions for the DAC plant: Two production cycles are required, running from t_1 to t_7 and from t_{15} to t_{21}, respectively (cf. Figs. 9(g) to (i)). In the simultaneous approach, the total CO_2 outputs of the two production cycles are 1324.7 kg and 673.6 kg, respectively. In contrast, the sequential and hybrid approaches identify identical outputs of 1304.9 kg and 686.8 kg per cycle. This difference increases the operational costs of the DAC plant by 24 EUR/d, thereby raising the total operational cost in the simultaneous approach. In addition, slight deviations between the energy and process system levels can be observed in the operational decisions for the DAC plant during time steps t_4 to t_7 (cf. Figs. 9(h) and (i)). These deviations arise because the convergence criterion for the DAC plant is defined as a cycle-based relative deviation of less than 3%. A stricter convergence criterion can be applied if necessary; however, it should be aligned with the convergence between the surrogate model and the detailed process model.

Different operational decisions of the MPs are mostly reflected in the operational decisions for the PEM electrolyzer (cf. Figs. 9(j) to (l)). The operational costs of the PEM electrolyzer via the sequential approach are slightly higher than the other two approaches (by 16 EUR/d), which is expected, as the first element in the list $\mathbf{K}^{\mathrm{PS}}$ (addressed in the final sequence) possesses relatively low operational flexibility. Nevertheless, the operational decisions for the PEM electrolyzer across the three solution approaches are quite similar. Since the PEM electrolyzer is an electricity-intensive consumer, electricity prices play a predominant role in its operational decisions.

Furthermore, to provide an intuitive insight into the convergence performance, Fig. 10 shows the sum of absolute deviations in the product output flows between the energy and process system levels of the PEM electrolyzer ($e = H_2$), the DAC plant ($e = CO_2$), and the MPs ($e = CH_4$) across 24 time steps for all three solution approaches. A more detailed visualization of the convergence evolution is available in the Supporting Information. Note that the method becomes effective from the third iteration for computing the estimation term, once at least one of the MPs is included in the current sequence (cf. lines 20 to 30 in Algorithm 1).

The largest absolute deviation in the simultaneous approach (cf. Fig. 10(a)) is below 400 units (kW for H_2 and CH_4, and kg/h for CO_2), whereas it reaches 600 units in the other two approaches (cf. Figs. 10(b) and (c)). In addition, the interaction among energy system components is more apparent when they are addressed simultaneously. For example, the absolute deviations for the MPs in Fig. 10(a) increase in the fifth iteration after decreasing in the fourth, aiding the convergence of the DAC plant. Similar interactions are also evident in Fig. 10(c) regarding the convergence of the MPs.

In contrast, the absolute deviations in the sequential approach vary more independently for each energy system component. For instance, the operational decisions for the MP2 in Fig. 10(b) exhibit significant variations despite ultimately achieving convergence. In the sixth iteration, only one decision variable (at the 11th time step) fails to meet the convergence condition, with a relative deviation of 3.8%. Then, in the next iteration, two new decision variables (at the 12th and 20th time steps) fail to meet the convergence condition, causing the relative deviations to increase dramatically to 20.3%.

Among all three approaches, the PEM electrolyzer consistently meets the convergence condition because its operational problem at each time step is fully independent. In contrast, the DAC plant, due to its multistage

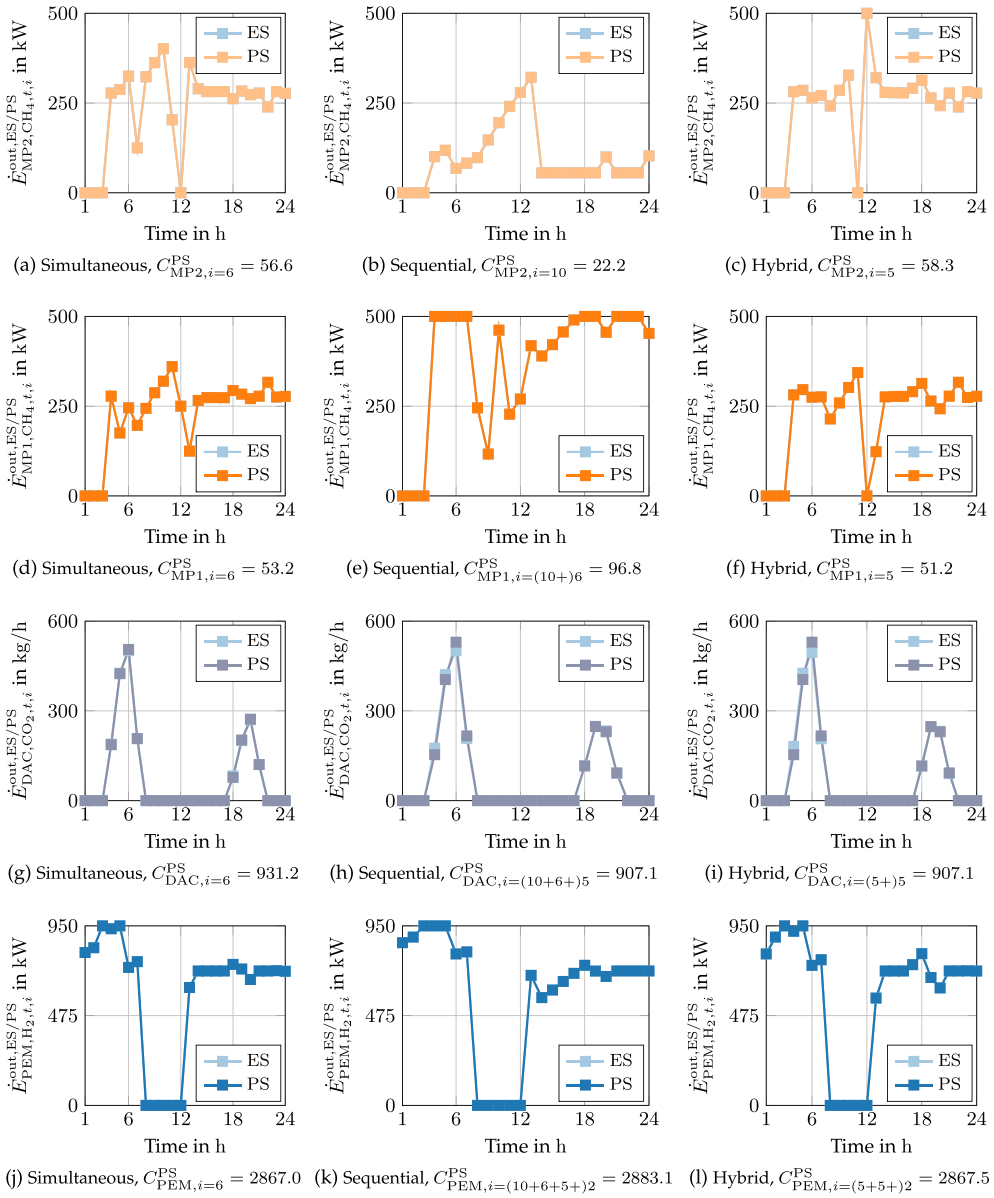

Fig. 9. Product output flows of the MP2 (first row), the MP1 (second row), the DAC plant (third row), and the PEM electrolyzer (fourth row) are shown for the simultaneous (left column), sequential (middle column), and hybrid (right column) approaches at both the energy (ES) and process system levels (PS). $C^{PS}_{k,i}$ denotes the operational costs of energy system component k in iteration i at the process system level, given in euros per day.

process characteristics, and the MPs, because of the presence of ramping constraints, do not share this independence. While the MPs exhibit dramatic changes across iterations, the iterations for determining the DAC plant's operational decisions (after the second iteration) resemble more of a fine-tuning process.

Overall, approximately 2% of the total operational cost of the power-to-X energy system is attributed to the MPs, around 16% to the DAC plant, and about 50% to the PEM electrolyzer. The proposed method effectively solves the complex operational optimization problems using three different solution approaches, each with varying computational performance. While the total operational costs across the three solution approaches are comparable, the computing times differ significantly. The hybrid approach effectively combines the strengths of both the simultaneous and sequential approaches. By balancing problem complexity, it achieves the lowest total operational cost and the highest computational efficiency, outperforming the other two approaches. Nevertheless, the high potential of the hybrid approach is closely tied to the structure of the energy system under consideration. In the applied power-to-X energy system, alternative setups, such as $\mathbf{K}^{PS} = \left[\text{PEM}, \left[\text{DAC}, \text{MP1}\right], \text{MP2}\right]$ or $\mathbf{K}^{PS} = \left[\left[\text{PEM}, \text{DAC}\right], \text{MP1}, \text{MP2}\right]$ can also be considered. In this work, we intuitively choose the setup $\mathbf{K}^{PS} = \left[\text{PEM}, \text{DAC}, \left[\text{MP1}, \text{MP2}\right]\right]$, since the two MPs can operate in parallel as long as the required CH_4 demand is met. A detailed investigation of the best setup of $\mathbf{K}^{PS}$ for the case study, however, is not conducted in this work.

4.4.2. Part B results: sensitivity study

The proposed decomposition method relies mainly on a penalty term to control the convergence of optimization problems between the energy and process system levels. So far, the presented results are all based on the scale factors $\gamma_{k,e}$ specified in Table 6. In the following, we conduct a sensitivity study to evaluate the impact of these scale factors in the penalty term on the overall method performance. As the

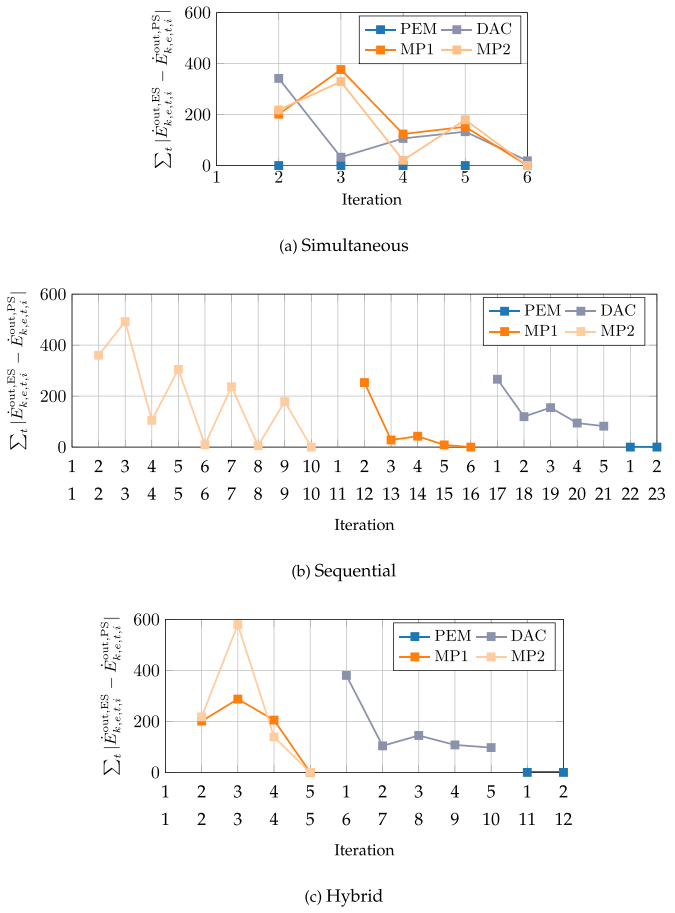

Fig. 10. Sum of absolute deviations between the energy (ES) and process system levels (PS) in the product output flows of the PEM electrolyzer ($e = H_2$), the DAC plant ($e = CO_2$), and the MPs ($e = CH_4$) across 24 time steps over iterations. Top: simultaneous approach; middle: sequential approach; bottom: hybrid approach.

simultaneous and sequential approaches represent the extremes of complexity introduced by the penalty term, this sensitivity study focuses on the simultaneous approach, which may involve the largest number of penalized decision variables, and the sequential approach, which may involve the fewest.

To do so, we uniformly adjust all previously used scale factor values by multiplying each by a common tuning coefficient κ. All other setups in Table 6 remain unchanged. We perform eight additional optimization computations with different tuning coefficients κ for each of the simultaneous and sequential approaches. The results are presented in Table 8. When the tuning coefficient κ equals 1, the results align with those analyzed earlier.

The presented results include the number of iterations at which the computation terminates (i_k^{term}), the final operational costs of each energy system component k at the process system level ($C^{\text{PS}}_{k,i=i_k^{\text{term}}}$), and the final total operational cost (C^{total}). Additionally, due to the varying orders of magnitude of decision variable values in our case study, the coefficient range of Problem (6) at the energy system level can be quite large. In case of numerical issues or an unsatisfied optimization gap reported by Gurobi, our method automatically recalculates Problem (6) with a higher value for the solver parameter `NumericFocus`, which corresponds to increased numerical stability. However, increasing the `NumericFocus` value also leads to higher computing time [49]. Therefore, we additionally track how often the solver parameter is reset (`NF`).

As shown in the middle column of Table 8, one of the nine optimization computations fails to converge when using the simultaneous approach (cf. $\kappa = 0.01$). This failure occurs because excessively small scale factors reduce the penalty term's impact on the objective function, thereby hindering the method's convergence. For instance, with $\kappa = 0.01$, the number of penalized decision variables reaches 49 by the eighth iteration and remains unchanged until the 14th iteration, at which point the 50th decision variable is added. These 50 decision variables remain in the objective function until the maximum number of iterations is reached. By the 17th iteration, the operational decisions for the PEM electrolyzer and the MPs have already converged. However, the operational decisions for the DAC plant remain infeasible throughout, ultimately rendering the operational problem for the entire energy system infeasible.

Another interesting computational result emerges when κ is set to 10 or 50. In these cases, the total operational costs are significantly higher than those in other computations. This is because the DAC plant operates with three cycles, leading to increased operational costs. For example, when $\kappa = 10$, a surplus of 432 kWh of CH_4 is produced via higher electricity prices and fed into the natural gas grid, where the CH_4 is sold at relatively low prices. In both cases, the excessively large scale factors, coupled with the strong interconnection of decision variables across time steps in a multistage batch process system and the large number of penalized decision variables (48 in the case of $\kappa = 10$), lead to an overemphasis of the penalty term in the objective function. This imbalance results in a sub-optimal solution.

The remaining six optimization computations converge to similar total operational costs, with the largest absolute difference being 20.5 EUR/d. Notably, the operational costs of the PEM electrolyzer and the MPs (the combined cost of the MP1 and MP2) are nearly identical across all six optimization computations. In contrast, slight variations in the operational cost of the DAC plant, up to 19 EUR/d, account for differences in the total operational costs.

Furthermore, the simultaneous approach generally requires long computing time. Only two of the nine cases complete the computations within one hour. The longest computing time even reaches 11 hours (cf. $\kappa = 50$). Additionally, half of the computations require a higher `NumericFocus` value at least once, which also explains their significantly high computing time.

The sensitivity study for the sequential approach is presented in the right column of Table 8. Similar to the simultaneous approach, when $\kappa = 0.01$, the operational decisions for the DAC plant at both the energy and process system levels do not converge after reaching the maximum number of iterations. However, in the sequential approach, we replace the surrogate models at the energy system level with the results from the process system level, regardless of whether $i_{\text{DAC}}^{\text{term}}$ exceeds $i^{\max}$ (cf. Eq. (11)). This ensures that the resulting operational decisions are still feasible, although not optimized, distinguishing it from the simultaneous approach. Subsequently, the operational decisions for the last energy system component, the PEM electrolyzer, are determined within two iterations. As a result, the sequential approach successfully yields a feasible operational strategy for the entire energy system in the case of $\kappa = 0.01$.

Moreover, the sequential approach generally identifies higher operational costs for the MP1, the DAC plant, and the PEM electrolyzer, and consequently higher total operational costs compared to the simultaneous approach (up to 42 EUR/d). However, in three cases ($\kappa = 0.05$, $\kappa = 1$, and $\kappa = 50$), the operational costs of the DAC plant are significantly lower, resulting in overall total operational costs that are even lower than those obtained using the simultaneous approach (about 18 EUR/d). In our case study, the optimization problems for the DAC plant in Part B are solved using a fast shortcut search path. The quality of the dataset $DS_{\text{DAC,CO}_2}$ and the effectiveness of the search strategy play crucial roles in determining the operational decisions. Since $DS_{\text{DAC,CO}_2}$ consists of the top 10 results obtained by solving optimization problems using a PSO genetic algorithm, slight variations in the operational decisions for the DAC plant is expected when different method setups are applied.

Table 8
Comparison of computing time, operational costs, and iteration counts for different tuning coefficients κ using the simultaneous and sequential approaches. i_k^{term} is the iteration where the algorithm terminated. `NF` indicates how many times the solver parameter `NumericFocus` was increased to improve numerical stability. The results for $\kappa = 1$ are presented in detail in the preceding subsections.

		Simultaneous approach					Sequential approach				
Tuning coefficient κ	Component k	i_k^{term}	$C^{\text{PS}}_{k,i=i_k^{\text{term}}}$	C^{total}	Computing time	NF	i_k^{term}	$C^{\text{PS}}_{k,i=i_k^{\text{term}}}$	C^{total}	Computing time	NF
0.01	PEM	20	2866.9	- [a]	11416	0	2	2900.9	5995.3	2811	0
	DAC	20 (2c, nC) [b]	-				10 (2c, nC) [b]	947.4			
	MP1	20	59.4				3	99.5			
	MP2	20	50.6				4	21.8			
0.05	PEM	8	2868.1	5960.2	6242	0	2	2878.2	5941.7	1810	0
	DAC	8	931.3				5	898.4			
	MP1	8	53.9				3	105.1			
	MP2	8	55.9				4	14.8			
0.1	PEM	12	2867.1	5979.2	12268	0	2	2882.8	5986.2	4210	0
	DAC	12	950.2				4	938.9			
	MP1	12	48.3				5	99.9			
	MP2	12	62.9				7	19.8			
0.5	PEM	7	2866.9	5959.1	21311	1	2	2878.7	5986.6	4113	0
	DAC	7	931.2				4	945.5			
	MP1	7	59.8				6	96.4			
	MP2	7	50.5				9	21.2			
1	PEM	6	2867.0	5958.7	3310	0	2	2883.1	5954.5	5040	0
	DAC	6	931.2				5	907.1			
	MP1	6	53.2				6	96.8			
	MP2	6	56.6				10	22.2			
5	PEM	6	2867.7	5959.8	3165	0	2	2913.5	5998.5	13733	1
	DAC	6	931.2				5	939.7			
	MP1	6	54.8				4	99.4			
	MP2	6	56.1				6	19.6			
10	PEM	10	3836.4	6859.2	28288	2	2	2889.0	6002.1	3372	0
	DAC	10	1312.7 (3c) [c]				4	945.4			
	MP1	10	75.3				5	93.8			
	MP2	10	73.9				5	28.3			
50	PEM	11	3523.6	6766.9	39707	2	2	2869.2	5941.4	13278	1
	DAC	11	1364.5 (3c) [c]				5	907.1			
	MP1	11	67.1				3	106.9			
	MP2	11	71.2				4	13.5			
100	PEM	7	2866.8	5960.8	4977	1	2	2876.8	5983.6	3099	0
	DAC	7	933.0				4	942.7			
	MP1	7	60.6				4	93.8			
	MP2	7	49.6				6	27.0			

[a] -: No feasible operational strategy is found.
[b] 2c, nC: Two cycles of the DAC plant did not converge.
[c] 3c: The DAC plant is operated with three cycles.

Compared to the simultaneous approach, the sequential approach demonstrates advantages in the computing time. Seven out of nine computations are completed within 1.5 hours, with the fastest taking only 30 minutes. The remaining two computations require relatively longer computing times (over 3 hours), due to the need for resetting the solver parameter `NumericFocus`.

In summary, both the simultaneous and sequential approaches can effectively solve the complex operational problem with properly chosen scale factors. The simultaneous approach is relatively sensitive to scale factors. Improperly chosen scale factors increase the solver's numerical precision requirements. While the simultaneous approach has the potential to identify solutions closest to the optimum, it comes at the expense of higher computing time. The sequential approach, on the other hand, is less sensitive to scale factors. In comparison, the sequential approach achieves faster computation but results in slightly higher total operational costs. Note that all total operational costs obtained in the sensitivity study are higher than those achieved using the hybrid approach discussed in the previous subsection.

5. Conclusions

This work proposes a decomposition method for solving operational optimization problems of renewables-based energy systems with detailed process models. Building on our previous work [31], which is limited to a single continuous process, this work extends the method to include multiple and more complex process models, including batch plants that involve multiple intricate processing stages.

We first introduce a surrogate modeling approach tailored to complex multistage processes in operational energy system optimization problems. Accordingly, the original complex operational optimization problem can be decomposed into an optimization problem at the energy system level, where the detailed process models are replaced by their corresponding surrogate models, and multiple optimization problems at the process system level, which directly employ the detailed process models.

Then, we propose three solution approaches (simultaneous, sequential, and hybrid) to solve the resulting decomposed optimization problems in an iterative manner. The algorithm iterates until the operational decisions at both the energy and process system levels, represented by surrogate and detailed process models, converge. This convergence is primarily controlled by a penalty term. The simultaneous approach considers all detailed process models simultaneously within each iteration, while the sequential approach solves the process models in a predefined order. The hybrid approach combines the simultaneous and sequential approaches, offering enhanced flexibility and computational efficiency.

We apply the decomposition method to optimize the daily operation of a power-to-X energy system comprising a PEM electrolyzer, a direct air capture (DAC) plant, and two identical methanation processes (MPs) operated in parallel. The PEM electrolyzer is represented as a continuous process system without ramping constraints, the MPs as continuous systems with ramping constraints, and the DAC plant as a multistage batch process system. The resulting operational optimization problem is solved using the simultaneous, sequential, and hybrid approaches. All three approaches yield comparable total operational costs, though with varying computing times. The hybrid approach outperforms the others by achieving the lowest total operational cost in the shortest computing time of 42 minutes.

A subsequent sensitivity study investigates the impact of scale factors in the penalty term on the performance of the simultaneous and sequential approaches. The simultaneous approach provides stable operational decisions and has the potential to identify the closest optima. However, it is more sensitive to the value of the scale factor, where inappropriate values can lead to infeasibility or sub-optimal solutions. Additionally, the simultaneous approach generally requires more computing time. In contrast, the sequential approach is much less sensitive to the value of the scale factor and can identify a feasible operational strategy in as little as 30 minutes. However, this approach tends to provide some variability in operational costs and is more prone to sub-optimal solutions.

In our work, the operational data applied for generating the surrogate models are locally optimal and near-optimal solutions. As a result, the final total operational cost exhibits slight variations (up to 0.5% in the simultaneous approach). In future work, global optimal solutions could be utilized if such detailed process models become available to enhance the precision of the results. Additionally, this work assumes a fixed cycle time duration for complex multistage process systems. In real-world applications, however, the time duration of a production cycle may vary depending on the initial conditions of the process system. If the change in cycle duration is negligible, i.e., the number of segments in the surrogate models remains unchanged, the proposed surrogate modeling approach would only need to incorporate the initial conditions of the process systems as input parameters. However, if the variations in cycle time duration cannot be ignored, the resulting surrogate models may involve disjunctive formulations (cf. Eqs. (2) and (5)), and more advanced techniques, such as machine learning-based surrogate models, may be required to accurately capture the input–output relationships of the process. Furthermore, the proposed method exhibits a strong dependence on the scale factors in the penalty term, which are selected heuristically in this work. Future efforts could focus on developing more efficient and systematic strategies for scale factor selection, such as using Bayesian optimization. Additionally, as the proposed method is heuristic, relaxation techniques could be further developed to provide a lower bound, thereby enabling an assessment of its optimality.

The proposed method can be readily scaled to accommodate more detailed process models (i.e., larger $\mathcal{K}^{\mathrm{PS}}$) and/or longer time horizons (i.e., larger $\mathcal{T}$). Although the computational burden may increase accordingly, the three proposed solution approaches provide alternative variants to effectively manage this complexity. Looking ahead, for very long time horizons, such as seasonal time scales, external uncertainty arising from the large time dimension should be considered in the operational optimization problems. In this context, the proposed method could be extended and integrated into stochastic or robust optimization techniques. Conversely, at finer temporal resolutions, such as minute-level time scales, the proposed method could be embedded within control strategies, for example, model predictive control, to enable real-world operational applications.

Overall, the proposed decomposition method addresses the challenge of solving operational optimization problems for energy systems with complex process models. It achieves a favorable balance between preserving model fidelity and ensuring computational efficiency. In light of the growing demand for innovation in energy systems, we anticipate that our method will be applicable to a broad range of renewables-based energy systems, particularly those integrating diverse variants of power-to-X technologies.

CRediT authorship contribution statement

Yifan Wang: Writing – original draft, Visualization, Software, Methodology, Investigation, Formal analysis, Data curation, Conceptualization. **Niklas von der Assen:** Writing – review & editing, Supervision, Funding acquisition, Conceptualization. **Qi Zhang:** Writing – review & editing, Supervision, Methodology, Formal analysis, Conceptualization.

Declaration of Generative AI and AI-assisted technologies in the writing process

During the preparation of this work, Y.W. used ChatGPT to improve readability and language. After using this tool, the authors reviewed and edited the content as needed and take full responsibility for the content of the publication.

Declaration of competing interest

The authors declare that they have no known competing financial interests or personal relationships that could have appeared to influence the work reported in this paper.

Acknowledgements

This study is co-funded by the “Europäischer Fonds für regionale Entwicklung” (EFRE-20800350) and a fellowship from the German Academic Exchange Service (DAAD). The support is gratefully acknowledged. Furthermore, we express our gratitude to Patrik Postweiler for providing the detailed process model of the direct air capture plant, Karan Anand and Marcelo Martinez Lluch for providing the detailed process model of the proton exchange membrane electrolyzer.

Appendix A. Supplementary materials

Supplementary material for this article can be found online at doi:10.1016/j.apenergy.2026.128445.

Data availability

The data used in this study are subject to the following licenses and restrictions: The code is published under an MIT license and is publicly available in a Git repository: https://git-ce.rwth-aachen.de/ltt/ptg-es4. The detailed process model of the direct air capture (DAC) plant is restricted to the TLK and DYMOLA licenses. However, these licenses are not required when using the shortcut search path, as applied in our case study. The full dataset for the DAC plant (about 50 GB) is also provided

on Zenodo: https://doi.org/10.5281/zenodo.14860488. Moreover, the Gurobi solver requires a separate license. Further inquiries can be directed to the corresponding authors.

References

[1] Gabrielli P, Gazzani M, Martelli E, Mazzotti M. Optimal design of multi-energy systems with seasonal storage. Appl Energy 2018;219:408–24. https://doi.org/10.1016/j.apenergy.2017.07.142

[2] Wang Y, Bornemann L, Reinert C, von der Aßen N. A power-to-gas energy system: modeling and operational optimization for seasonal energy supply and storage. In: 33rd European symposium on computer aided process engineering, vol. 52. Elsevier; 2023. p. 2867–72. https://doi.org/10.1016/B978-0-443-15274-0.50456-X Computer Aided Chemical Engineering.

[3] Marzi E, Morini M, Saletti C, Vouros S, Zaccaria V, Kyprianidis K, Gambarotta A. Power-to-gas for energy system flexibility under uncertainty in demand, production and price. Energy 2023;284:129212. https://doi.org/10.1016/j.energy.2023.129212

[4] Zhang L, Jia C, Bai F, Wang W, An S, Zhao K, Li Z, Li J, Sun H. A comprehensive review of the promising clean energy carrier: hydrogen production, transportation, storage, and utilization (HPTSU) technologies. Fuel 2024;355:129455. https://doi.org/10.1016/j.fuel.2023.129455

[5] Mitsos A, Asprion N, Floudas CA, Bortz M, Baldea M, Bonvin D, Caspari A, Schäfer P. Challenges in process optimization for new feedstocks and energy sources. Comput Chem Eng 2018;113:209–21. https://doi.org/10.1016/j.compchemeng.2018.03.013

[6] Valera-Medina A, Amer-Hatem F, Azad AK, Dedoussi IC, de Joannon M, Fernandes RX, Glarborg P, Hashemi H, He X, Mashruk S, McGowan J, Mounaim-Rouselle C, Ortiz-Prado A, Ortiz-Valera A, Rossetti I, Shu B, Yehia M, Xiao H, Costa M. Review on ammonia as a potential fuel: from synthesis to economics. Energy Fuels 2021;35:6964–7029. https://doi.org/10.1021/acs.energyfuels.0c03685

[7] Fodstad M, Crespo Del Granado P, Hellemo L, Knudsen BR, Pisciella P, Silvast A, Bordin C, Schmidt S, Straus J. Next frontiers in energy system modelling: a review on challenges and the state of the art. Renew Sustain Energy Rev 2022;160:112246. https://doi.org/10.1016/j.rser.2022.112246

[8] Le TT, Sharma P, Bora BJ, Tran VD, Truong TH, Le HC, Nguyen PQP. Fueling the future: a comprehensive review of hydrogen energy systems and their challenges. Int J Hydrog Energy 2024;54:791–816. https://doi.org/10.1016/j.ijhydene.2023.08.044

[9] Mucci S, Mitsos A, Bongartz D. Power-to-X processes based on PEM water electrolyzers: a review of process integration and flexible operation. Comput Chem Eng 2023;175:108260. https://doi.org/10.1016/j.compchemeng.2023.108260

[10] Petkov I, Gabrielli P. Power-to-hydrogen as seasonal energy storage: an uncertainty analysis for optimal design of low-carbon multi-energy systems. Appl Energy 2020;274:115197. https://doi.org/10.1016/j.apenergy.2020.115197

[11] Zhang X, Zhang Y. Environment-friendly and economical scheduling optimization for integrated energy system considering power-to-gas technology and carbon capture power plant. J Clean Prod 2020;276:123348. https://doi.org/10.1016/j.jclepro.2020.123348

[12] Rönsch S, Schneider J, Matthischke S, Schlüter M, Götz M, Lefebvre J, Prabhakaran P, Bajohr S. Review on methanation – from fundamentals to current projects. Fuel 2016;166:276–96. https://doi.org/10.1016/j.fuel.2015.10.111

[13] Dieterich V, Buttler A, Hanel A, Spliethoff H, Fendt S. Power-to-liquid via synthesis of methanol, DME or fischer–tropsch-fuels: a review. Energy Environ Sci 2020;13:3207–52. https://doi.org/10.1039/D0EE01187H

[14] Wulf C, Linßen J, Zapp P. Review of power-to-gas projects in Europe. Energy Procedia 2018;155:367–78. https://doi.org/10.1016/j.egypro.2018.11.041

[15] Gabrielli P, Flamm B, Eichler A, Gazzani M, Lygeros J, Mazzotti M. Modeling for optimal operation of PEM fuel cells and electrolyzers. In: 2016 IEEE 16th international conference on environment and electrical engineering (EEEIC). IEEE; 2016. p. 1–7. https://doi.org/10.1109/EEEIC.2016.7555707

[16] Baader FJ, Bardow A, Dahmen M. MILP formulation for dynamic demand response of electrolyzers. In: 14th international symposium on process systems engineering, vol. 49. Elsevier; 2022. p. 391–6. https://doi.org/10.1016/B978-0-323-85159-6.50065-8 Computer Aided Chemical Engineering.

[17] Fasihi M, Efimova O, Breyer C. Techno-economic assessment of CO_2 direct air capture plants. J Clean Prod 2019;224:957–80. https://doi.org/10.1016/j.jclepro.2019.03.086

[18] Andrés-Martínez O, Zhang Q, Daoutidis P. Optimal operation of a reaction-absorption process for ammonia production at low pressure. Ind Eng Chem Res 2023;62:14456–66. https://doi.org/10.1021/acs.iecr.3c01679

[19] Andrés-Martínez O, Malmali M, Zhang Q, Daoutidis P. Optimal design of an absorbent-enhanced ammonia synthesis process for solar thermochemical energy storage. ACS Sustain Chem Eng 2024;12:9446–60. https://doi.org/10.1021/acssuschemeng.4c02464

[20] Cheng Y, Liu M, Chen H, Yang Z. Optimization of multi-carrier energy system based on new operation mechanism modelling of power-to-gas integrated with CO_2-based electrothermal energy storage. Energy 2021;216:119269. https://doi.org/10.1016/j.energy.2020.119269

[21] Wu Q, Li C. Modeling and operation optimization of hydrogen-based integrated energy system with refined power-to-gas and carbon-capture-storage technologies under carbon trading. Energy 2023;270:126832. https://doi.org/10.1016/j.energy.2023.126832

[22] Baader FJ, Bardow A, Dahmen M. Simultaneous mixed–integer dynamic scheduling of processes and their energy systems. Aiche J 2022;68. https://doi.org/10.1002/aic.17741

[23] Baader FJ, Althaus P, Bardow A, Dahmen M. Dynamic ramping for demand response of processes and energy systems based on exact linearization. J Process Control 2022;118:218–30. https://doi.org/10.1016/j.jprocont.2022.08.017

[24] Baader FJ, Althaus P, Bardow A, Dahmen M. Demand response for flat nonlinear MIMO processes using dynamic ramping constraints. Comput Chem Eng 2023;172:108171. https://doi.org/10.1016/j.compchemeng.2023.108171

[25] Bornemann L, Lange J, Kaltschmitt M. Optimizing temperature and pressure in PEM electrolyzers: a model-based approach to enhanced efficiency in integrated energy systems. Energy Convers Manag 2025;325:119338. https://doi.org/10.1016/j.enconman.2024.119338

[26] Papadimitriou C, Baldea M, Mitsos A. Dynamic scheduling: a comparison of high-fidelity models with local optimization versus surrogate models with global optimization. Ind Eng Chem Res 2025;64:21641–57. https://doi.org/10.1021/acs.iecr.5c02705

[27] Kotzur L, Nolting L, Hoffmann M, Groß T, Smolenko A, Priesmann J, Büsing H, Beer R, Kullmann F, Singh B, Praktiknjo A, Stolten D, Robinius M. A modeler's guide to handle complexity in energy systems optimization. Adv Appl Energy 2021;4:100063. https://doi.org/10.1016/j.adapen.2021.100063

[28] Ramanujam A, Li C. A tutorial on multi-time scale optimization models and algorithms, arXiv preprint arXiv:2502.20568. 2025.

[29] Elsido C, Martelli E, Grossmann IE. A bilevel decomposition method for the simultaneous heat integration and synthesis of steam/organic rankine cycles. Comput Chem Eng 2019;128:228–45. https://doi.org/10.1016/j.compchemeng.2019.05.041

[30] Jiménez-Romero J, Azapagic A, Smith R. BEELINE: BilevEl dEcomposition aLgorithm for synthesis of industrial eNergy systEms. Comput Chem Eng 2024;180:108406. https://doi.org/10.1016/j.compchemeng.2023.108406

[31] Wang Y, Bornemann L, Reinert C, von der Assen N. A method to bridge energy and process system optimization: identifying the feasible operating space for a methanation process in power-to-gas energy systems. Comput Chem Eng 2024;182:108582. https://doi.org/10.1016/j.compchemeng.2023.108582

[32] Conejo AJ, Castillo E, García-Bertrand R, Mínguez R. Decomposition techniques in mathematical programming: engineering and science applications. Berlin: Springer; 2006. https://doi.org/10.1007/3-540-27686-6

[33] Constante-Flores GE, Conejo AJ. Optimization via relaxation and decomposition. vol. 364. Cham: Springer Nature Switzerland; 2025. https://doi.org/10.1007/978-3-031-87405-5

[34] Iyer RR, Grossmann IE. A bilevel decomposition algorithm for long-range planning of process networks. Ind Eng Chem Res 1998;37:474–81. https://doi.org/10.1021/ie970383i

[35] Buttler A, Spliethoff H. Current status of water electrolysis for energy storage, grid balancing and sector coupling via power-to-gas and power-to-liquids: a review. Renew Sustain Energy Rev 2018;82:2440–54. https://doi.org/10.1016/j.rser.2017.09.003

[36] Postweiler P, Engelpracht M, Rezo D, Gibelhaus A, von der Assen N. Environmental process optimisation of an adsorption-based direct air carbon capture and storage system. Energy Environ Sci 2024;17:3004–20. https://doi.org/10.1039/D3EE02970K

[37] Wang Y. PtG-ES4: power-to-gas energy systems for seasonal energy supply and storage. 2023. https://git-ce.rwth-aachen.de/ltt/ptg-es4 [Accessed 17 April 2026].

[38] Anand K, Kelm J, Reinert C, von der Assen NV. Dynamic modelling of PEM electrolyzers for flexible operation using artificial neural networks; 2022. https://publications.rwth-aachen.de/record/855674.

[39] Rezo D, Postweiler P, Engelpracht M, Meuleneers L, von der Aßen N. A method for siting adsorption-based direct air carbon capture and storage plants for maximum CO_2 removal. Carbon Neutrality 2024;3:26. https://doi.org/10.1007/s43979-024-00100-z

[40] Langiu M, Shu DY, Baader FJ, Hering D, Bau U, Xhonneux A, Müller D, Bardow A, Mitsos A, Dahmen M. COMANDO: a next-generation open-source framework for energy systems optimization. Comput Chem Eng 2021;152:107366. https://doi.org/10.1016/j.compchemeng.2021.107366

[41] Beal LDR, Hill DC, Martin RA, Hedengren JD. GEKKO optimization suite. Processes 2018;6:106. https://doi.org/10.3390/pr6080106

[42] Lee A, Ghouse JH, Eslick JC, Laird CD, Siirola JD, Zamarripa MA, Gunter D, Shinn JH, Dowling AW, Bhattacharyya D, Biegler LT, Burgard AP, Miller DC. The IDAES process modeling framework and model library—flexibility for process simulation and optimization. J Adv Manuf Process 2021;3:1. https://doi.org/10.1002/amp2.10095

[43] FMI standard. Funtional mock-up interface. 2022. https://fmi-standard.org [Accessed 19 April 2025].

[44] Gurobi Optimization, LLC. Gurobi optimizer reference manual. 2024. https://www.gurobi.com [Accessed 19 April 2025].

[45] Wächter A, Biegler LT. On the implementation of an interior-point filter line-search algorithm for large-scale nonlinear programming. Math Program 2006;106:25–57. https://doi.org/10.1007/s10107-004-0559-y

[46] Blank J, Deb K. Pymoo: multi-objective optimization in Python. IEEE Access 2020;8:89497–509. https://doi.org/10.1109/ACCESS.2020.2990567

[47] Zhang Q, Grossmann IE, Sundaramoorthy A, Pinto JM. Data-driven construction of convex region surrogate models. Optim Eng 2016;17:289–332. https://doi.org/10.1007/s11081-015-9288-8

[48] Pedregosa F, Varoquaux G, Gramfort A, Michel V, Thirion B, Grisel O, Blondel M, Prettenhofer P, Weiss R, Dubourg V, Vanderplas J, Passos A, Cournapeau D, Brucher M, Perrot M, Duchesnay E. Scikit-Learn: machine learning in Python. J Mach Learn Res 2011;12:2825–30. http://jmlr.org/papers/v12/pedregosa11a.html.

[49] Gurobi Optimization, LLC. Parameter reference. 2024. https://docs.gurobi.com/projects/optimizer/en/11.0/reference/parameters.html [Accessed 19 April 2025].